Report for Kystverket

Update of the 2019 Site-Specific Seismic Hazard Study for submarine U-864 location

May 2026

Stiftelsen NORSAR

P.O. Box 53, NO-2027 Kjeller, Norway

NORSAR

Contents

Executive summary

This report presents an update of the 2019 site-specific probabilistic seismic hazard assessment (PSHA) for the U-864 wreck location west of Fedje (NORSAR, 2019). The update was requested by Kystverket in February 2026 to incorporate recent developments in seismic hazard in the last seven years, including the update of the national seismic hazard model for Norway and Svalbard, additional recorded seismicity, revised ground-motion prediction equations (GMPEs), and methodological experience gained through recent NORSAR offshore hazard studies.

The updated assessment maintains the overall modelling framework of the 2019 study in order to allow direct comparison of results, while revising the main model components for which new data or methods are available. These include the regional earthquake catalogue (updated to end-February 2026), magnitude of completeness, seismic zonation, recurrence parameters, maximum magnitude assumptions, the GIS-based hazard model, and the GMPE logic tree. The hazard calculations were also recomputed for reference rock conditions corresponding to Vs30 = 1200 m/s.

Compared with the 2019 study, the updated results show generally higher hazard levels, particularly at short periods (see table below). The increase is primarily driven by the updated logic tree, which includes a broader set of Ground Motion Prediction Equations that predict higher ground motions at short periods and better capture epistemic uncertainty. The largest increases are observed for Peak Ground Acceleration (PGA) and short-period Spectral Acceleration (SA), while changes at longer periods are smaller and, in some cases, slightly lower than in 2019. For PGA, the updated values are 25.2 cm/s^2, 97.3 cm/s^2, and 465 cm/s^2 for return periods of 100, 475, and 10,000 years, respectively, compared with 17 cm/s^2, 72 cm/s^2, and 367 cm/s^2 in the 2019 study. Overall, the updated results confirm the general hazard pattern identified in 2019 but indicate moderately higher short-period ground-motion levels at the U-864 site.

	Spectral acceleration (cm/s^2)					
	100 yr		475 yr		10,000 yr	
Period (s)	***2019***	***2026***	***2019***	***2026***	***2019***	***2026***
0.01 (PGA)	17	25.2	72	97.3	367	465
0.05	33	49	133	190	756	930
0.1	39	57.8	160	217	777	1010
0.2	31	42.4	130	155	605	684
0.5	14	16.8	70	69.1	358	309
1.0	6	6.63	35	33.2	195	158
1.5	3	3.57	20	20.1	115	101
2.0	2	2.25	14	13.7	82	70.3
3.0	1	1.14	7	7.54	46	40.5

1 Introduction

1.1 Background and objectives

In November 2019, NORSAR delivered the report “Site-Specific Seismic Hazard Study for the Submarine Wreck U-864 Location, Norway” to the Norwegian Coastal Administration (Kystverket). The objective of that study was to quantify the seismic hazard at the wreck location west of Fedje in order to support the engineering design of the supporting fill beneath the wreck sections and the capping solution intended to ensure long-term stability of the area (Figure 1-1).

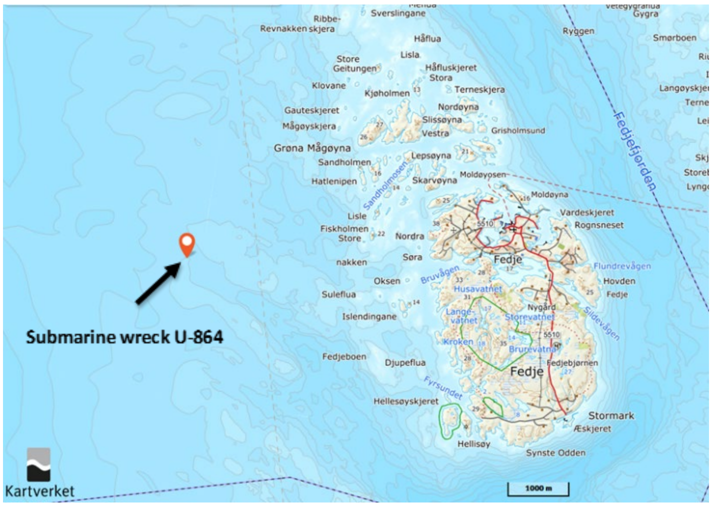

Figure 1-1: Location of the submarine wreck U-864 for which seismic hazard values are computed in this report. The wreck is located west of Fedje island in Hordaland.

The 2019 study was performed as a site-specific Probabilistic Seismic Hazard Analysis (PSHA), and the results were provided in terms of Peak Ground Acceleration (PGA) and Spectral Acceleration (SA) for return periods relevant for offshore structures.

Since the publication of the 2019 report (NORSAR, 2019), several developments relevant to seismic hazard assessment in Norway have taken place. These include the development of an updated national seismic hazard model for Norway and Svalbard (released in 2019 and subsequently documented by Lindholm et al. (2025)), the occurrence of additional recorded seismic events, and the availability of revised Ground Motion Prediction Equations (GMPEs) based on expanded strong-motion datasets. In addition, NORSAR has recently conducted several site-specific seismic hazard studies for offshore projects (NORSAR, 2025, 2022), providing further methodological experience and the application of updated datasets and modelling approaches.

In February 2026, Kystverket requested an update of the 2019 seismic hazard study in order to incorporate these developments. The objective of the present study is therefore to update the site-specific probabilistic seismic hazard assessment for the U-864 wreck location using updated seismic data, revised ground-motion models, and current methodological practices, while maintaining consistency with the modelling framework established in the 2019 study. This approach allows direct comparison between the updated results and the hazard estimates previously reported.

1.2 Scope of work and updated PSHA model

The present study consists of a targeted update of key components of the PSHA model developed in the 2019 study. The update focuses on incorporating new data and methodological improvements while retaining those aspects of the original model that remain valid for the U-864 region. The overall probabilistic framework, including source characterization, recurrence modelling, and logic-tree treatment of epistemic uncertainty, follows the approach adopted in the 2019 report. The main updates carried out in this study include:

- Updating the regional earthquake catalogue to include events recorded up to early 2026 and reassessing the magnitude of completeness.
- Re-estimating earthquake recurrence parameters for the newly defined seismic source regions and reviewing maximum magnitude (Mmax) assumptions.
- Updating Ground Motion Prediction Equations (GMPEs) relevant for the Norwegian offshore region.
- Recomputing PSHA results at the U-864 wreck location.

Hazard calculations have been performed using the R-CRISIS software (updated to version 20.3.0) and are expressed in terms of Peak Ground Acceleration (PGA), Spectral Acceleration (SA), and Uniform Hazard Spectra (UHS) for return periods of 100, 475, and 10,000 years. In this update, hazard results are computed for reference rock conditions corresponding to Vs30 = 1200 m/s, consistent with recent NORSAR offshore studies.

The update does not involve a fundamental revision of the general probabilistic seismic hazard assessment (PSHA) methodology and the geological/ seismotectonic framework established in the 2019 study. Instead, only those model components for which new data or methodological developments are available have been revised (Table 1-1), allowing direct comparison with previously reported hazard estimates.

Table 1-1: Overview of PSHA model components, associated report chapters, and their status in the present study relative to the 2019 assessment.

Model component	**Report chapter**	**Status**
General PSHA methodology	2	unchanged
Geological/seismotectonic setting	3	unchanged
GIS project	/	updated
Earthquake catalogue	4.1	updated to 2026
Seismic zonation	4.1	updated
Recurrence parameters	4.1	updated
Mmax	4.1	reviewed
GMPEs	4.2	updated
Hazard computation	5	recomputed

2 Technical approach

The documentation in this section is general and allows a practicing engineer to understand the main principles and methods that have been applied in the present Probabilistic Seismic Hazard Analysis (PSHA).

2.1 Design codes and return periods

The selection of the appropriate hazard level is essentially a question of the consequences of a structural failure. The hazard level is specified either as an annual exceedance probability or as an exceedance probability during the expected lifetime of the structure for a given ground motion intensity. Curves of various probabilities of exceedance as a function of a structure's life time and return period are shown in Figure 2-1.

The discussion of risk levels is supported through the following relationship between return period T_R and lifetime T, where P is the annual probability of exceedance (see Figure 2-1):

$$T_R = \frac{-T}{\ln(1 - P(Z > z))}$$

If, for example, the expected lifetime of a structure is T = 200 years, and a 95% non-exceedance probability (i.e., 5% exceedance probability, $P(Z>z)$ = 0.05) is required, then this safety requirement corresponds to a return period of T_R = 3899 years, or an equivalent annual exceedance probability of $2.564 \cdot 10^{-4}$. The results presented in this investigation reflect on three different return periods: of 40% exceedance probability in 50 years (100 years return period); 10% exceedance probability in 50 years (475 years return period); and 1% exceedance probability in 100 years. The 475 years return period is the hazard level required under Eurocode 8 for normal structures (importance class II) on the Norwegian mainland, whereas for offshore structures, 100 and 10,000 years return periods are required (NORSOK N-003, 2017). The long return periods (as 10,000 years) are used for critical infrastructures, like nuclear power plants, dams, and also for offshore structures. In this case, we provide seismic hazard results for 10,000 years also because the study area is exposed to the risk of mercury leakage that can have a negative environmental impact. The earthquake loading for 10,000 years return period was also used in the previous study (GeoPartner AS, 2010) to design the capping. In our opinion, we provide seismic hazard results for 100, 475 and 10,000 years return periods also to have a direct comparison between the actual site-specific seismic hazard study for the U-864 location and the previous NORSAR and NGI (1998) investigation.

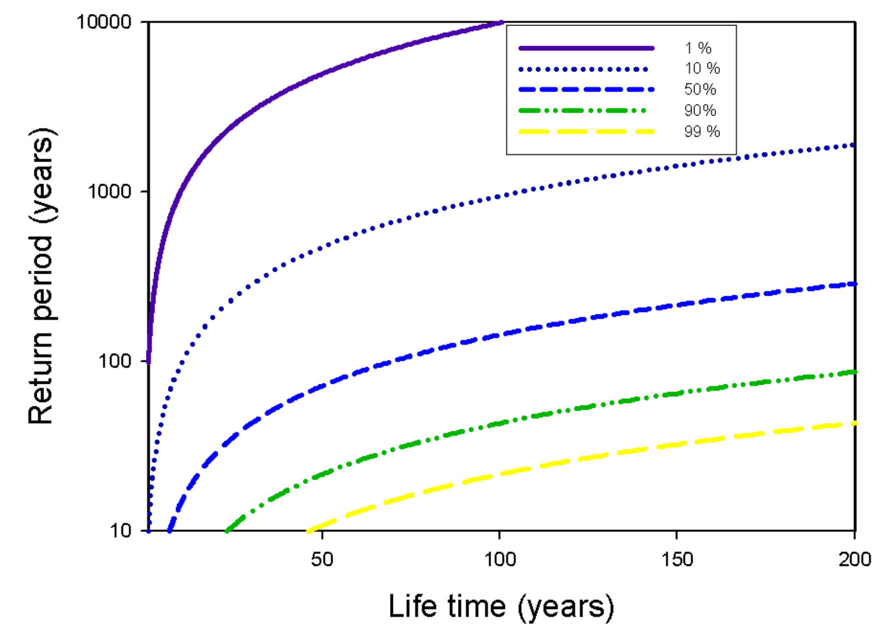

Figure 2-1: Relationship between return periods (inverse of annual exceedance probability), life time (or period of interest) and desired probability of exceedance (legend) during the period of interest (Reiter, 1990).

2.2 Methodology of Probabilistic Seismic Hazard Analysis (PSHA)

It is well known that uncertainties are essential in the definition of all elements that go into seismic hazard analysis, in particular since the uncertainties often drive the results, and increasingly so for low-exceedance probabilities. As might be anticipated this can sometimes lead to difficult choices for decision makers. Rational solutions to dilemmas posed by uncertainty can be based on the utilization of some form of probabilistic seismic hazard analysis (PSHA). In contrast to the typical deterministic analysis, which (in its simplest form) makes use of discrete single-valued events or models to arrive at the required description of earthquake hazard, PSHA allows the use of multi-valued or continuous model parameters. It is of major importance that the probabilities of different magnitudes or intensity earthquakes are included in the analysis. Another advantage of PSHA is that the results can be applied to estimate the likelihood of earthquake damage occurring at the location to a given structure of interest. This allows for a more sophisticated incorporation of seismic hazard into seismic risk estimates.

The methodology of probabilistic seismic hazard analysis (PSHA) was first defined by Esteva (1963) and Cornell (1968). There are four basic steps for the conduct of an PSHA:

- **Step 1** is the definition of earthquake sources. Sources may range from faults (small or large) to large seismotectonic provinces with uniform seismicity.
- **Step 2** is the definition of seismicity recurrence characteristics for the sources, where each source is described by an earthquake probability distribution, or recurrence relationship. A recurrence relationship indicates the chance of an earthquake of a given size to occur anywhere

inside or at the source during a specified period of time. A maximum or upper bound earthquake is chosen for each source, which represents the maximum magnitude to be considered. Because these earthquakes are assumed to occur anywhere within the earthquake source region, distances from all possible locations within the respective source to the site must be considered.

- **Step 3** is the estimation of ground motion intensity as a function of magnitude, distance and spectral period, where the range of earthquake sizes considered requires a selection of earthquake ground-motion attenuation relations (formally called Ground-Motion Prediction Equations GMPEs), each relating to a ground motion intensity parameter, such as peak ground acceleration or spectral acceleration.
- **Step 4** is the determination of the hazard at the site, which is substantially dissimilar from the procedure of deterministic hazard. In this case the effects of all the earthquakes of different sizes occurring at different locations in different earthquake sources at different probabilities of occurrence are integrated into one curve that shows the probability of exceeding different levels of seismic ground motion (such as peak ground acceleration) at the site during a specified period of time. With some assumptions this can be expressed as:

$$E(Z) = \sum_{i=1}^{N} \alpha_i \int_{m_o}^{m_u} \int_{r=0}^{r_{\max}} P(Z > z \mid m, r)\, f_{M_i}(m)\, f_{R_i}(r)\, dr\, dm$$

where *E(Z)* is the expected number of exceedances of ground motion intensity *z* during a specified time period *t*, α_i is the mean rate of occurrence of earthquakes between lower and upper bound magnitudes (m_o and m_u), f_{Mi} (m) is the probability density distribution of magnitude within the source *i*, $f_{Ri}(r)$ is the probability density distribution of epicentral distance between the various locations within source *i* and the site for which the hazard is being estimated, and $P(Z > z \mid m, r)$ is the probability that a given earthquake of magnitude m and epicentral distance *r* will exceed ground motion level *z*.

When conducting a PSHA it is usually assumed that earthquakes are Poisson-distributed and therefore have no ”memory”. This implies that each earthquake occurs independently of any other earthquake, and hence fore- and after-shocks are excluded in the statistical analysis.

2.3 Uncertainties

It is well known that uncertainties are intrinsic in the definition of all elements that go into seismic hazard analysis and, for low-exceedance probabilities, the uncertainties often strongly influence results. As might be anticipated, this can sometimes lead to difficult choices for decision makers. The PSHA implementation in logic tree schemes allows the use of multi-valued or continuous model parameters to be fully included in the analysis.

The observational period of earthquake activity in Norway and surrounding regions essentially covers around 130 years. This means that reliable and quantifiable earthquake information does not stretch as far back in history as for many other countries. Since the return periods of large and damaging earthquakes are much longer than this short observational period, it becomes clear that the uncertainty of any hazard estimate will be significant. This uncertainty is much more important when the results need to be given with very low annual exceedance probabilities. In every part of the assessment process uncertainty is quantified and carried through the PSHA computations. Sources of the uncertainties are schematically illustrated in Figure 2-2.

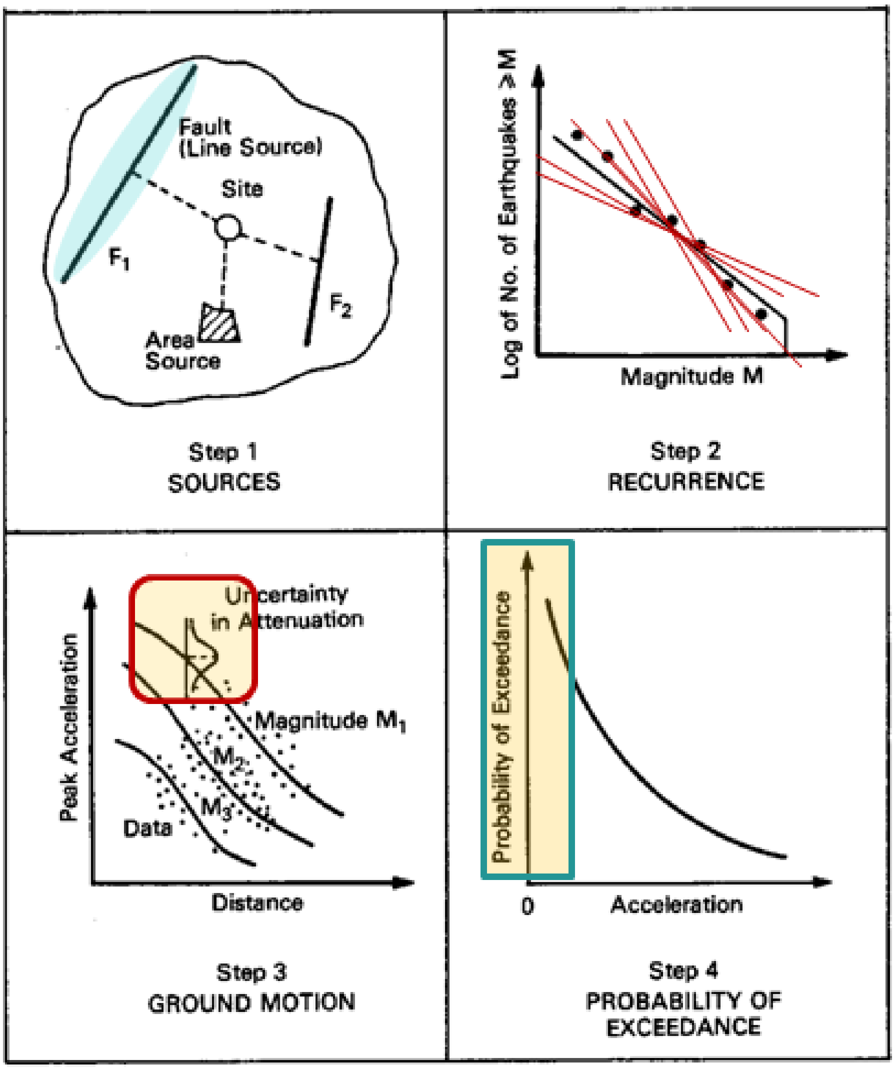

Figure 2-2: Illustration of the principal model uncertainties that are carried through the PSHA modelling: The area definition and the alternative fault line definition, the magnitude-frequency quantification and the ground motion prediction equation (GMPE) as a function of distance, magnitude and frequency. This parameterization uncertainty leads to uncertainty in the exceedance probability calculations.

2.4 Software used for the calculation

A number of computer codes have been developed and are available as free or as commercial software. For the present calculations, the R-CRISIS software has been applied (Ordaz et al., 2021, 2013). This code implements the probabilistic principles and is today regarded as being among the most advanced codes available. The major advantage of the CRISIS software over other software is its flexibility with respect to recurrence model parameterization and the integration procedure.

2.5 Procedure followed for the present study

The earthquake loading criteria developed in this study are based on PSHA techniques, configured to incorporate uncertainties and to quantify variability in the final hazard characterizations. The procedure for identifying potential seismic sources in the project region comprises the following basic steps:

- **Geology:** The general approach here is to review relevant and available geological information in order to locate and characterize seismically active and potentially active geological structures.
- **Seismology:** A seismic hazard analysis is largely based on the seismological history of the region, including recent and historical seismicity, supplemented with paleo-seismological information, if available. Essentially, the evidential worth of this data depends on the quality of the earthquake catalogue used. For this reason, a significant effort is spent to analyse the earthquake catalogue.
- **Seismotectonics:** The geological and seismological information is used to define models for the potential earthquake sources that could influence the hazard at the site. The main aspects of the source characterization are to model area sources based on the geologic history of the region in general (and on earthquake occurrence statistics in particular), and fault-specific sources with three-dimensional geometry, if such detailed information is available.
- **Ground motion attenuation models:** The present earthquake hazard study requires the availability of suitable GMPE models for peak ground acceleration and spectral accelerations. These relations are used to predict the ground motion intensity from a given magnitude at a given distance.
- **Computational model:** The actual seismic hazard computations for a specific site are based on a computational model that integrates all model parameters, usually with an integrated logic tree formulation. The uncertainties of the input parameters are carried through the computation.
- **Seismic hazard and loading results:** The final outcome of the above analysis and computation model leads to the hazard results in terms of Uniform Hazard Spectra (UHS) for specific sites.

We emphasize that a PSHA methodology was also applied in the earlier NORSAR and NGI (1998) investigation. Since then, significant advances have been made through the incorporation of improved scientific understanding, expanded datasets, and developments in computational methods. These advances are reflected in more recent studies, including updated national-scale seismic hazard assessments (Lindholm et al., 2025; NORSAR, 2020) as well as several site-specific PSHA investigations (NORSAR, 2025, 2022). Consequently, in light of improved scientific understanding and more data, as well as developments in software implementation, the present investigation can be regarded as fundamentally new work, and the results are consequently distinct from the previous NORSAR and NGI (1998) findings.

3 Geological and seismotectonic settings

In this chapter, a description of the most important geological structures and the seismotectonic overview around the study area are presented.

3.1 Regional geological setting

The main structural elements of Norway are the result of the orogenic events that welded the continent together (Figure 3-1). The larger blocks of present-day south-eastern Norway were formed during the Caledonian Orogeny. During this time period, microcontinents that were moving eastward collided with each other successively, thrusting the western blocks over the eastern blocks. This large overthrust from the west created the northern and southern mylonite zones, which are now revealed as N-S trending and steeply SW dipping lineaments. Rocks from the Caledonian Orogeny cover large parts of Norway. This episode of continental collision involved transport toward the east of earlier continental fragments and rifts, with very significant continental shortening. These mylonite zones are still today represented as N-S trending weakness zones, running through all of Norway and the shelf regions (Figure 3-1).

In Figure 3-1 a closer view on the south-middle Norwegian shelf is shown and it is possible to recognize the major fault systems, structural elements and the basin distribution of the northern North Sea.

Below there is a description of the principal structures that are close to the study region: the Viking Graben, the Hardangerfjorden shear zone, the Øygarden Fault Zone and the Nordfjord-Sogn detachment.

<u>Viking Graben</u>

The western Viking Graben boundary fault (WVGBF) marks the eastern boundary of the Shetland Platform from 58.5° N and NW-SE up to about 61.5° N where the northern North Sea trends are interrupted by the eastern marginal faults of the Færøy-Shetland Basin. During the Mesozoic, the pattern of displacement was generally associated with the regional rifting seen throughout the northern North Sea. Two episodes of rifting have been identified during the Paleocene associated with the uplift of the Shetland Platform. Following the Paleocene, the WVGBF continued to act as a hinge line between the stable Shetland Platform and the subsiding northern North Sea Basins (Wood and Woo, 1987).

<u>Hardangerfjorden shear zone</u>

The Hardangerfjorden shear zone is one of the largest tectonic structures in Norway. Fjords tend to form in zones of weakness in the crust, and this large shear zone is located in the crust beneath the Hardangerfjorden. The Hardangerfjorden shear zone is a low-angled extensional structure that stretches for more than 600 km. It was formed during continued extension of the crust that caused a shear zone that affects the orogenic wedge in addition to the basement (Fossen and Hurich, 2005). Deep seismic studies have shown that the shear zone reaches as deep as the lower crust at approximately 20-25 km with a dip of 22-23° (Fossen and Hurich, 2005).

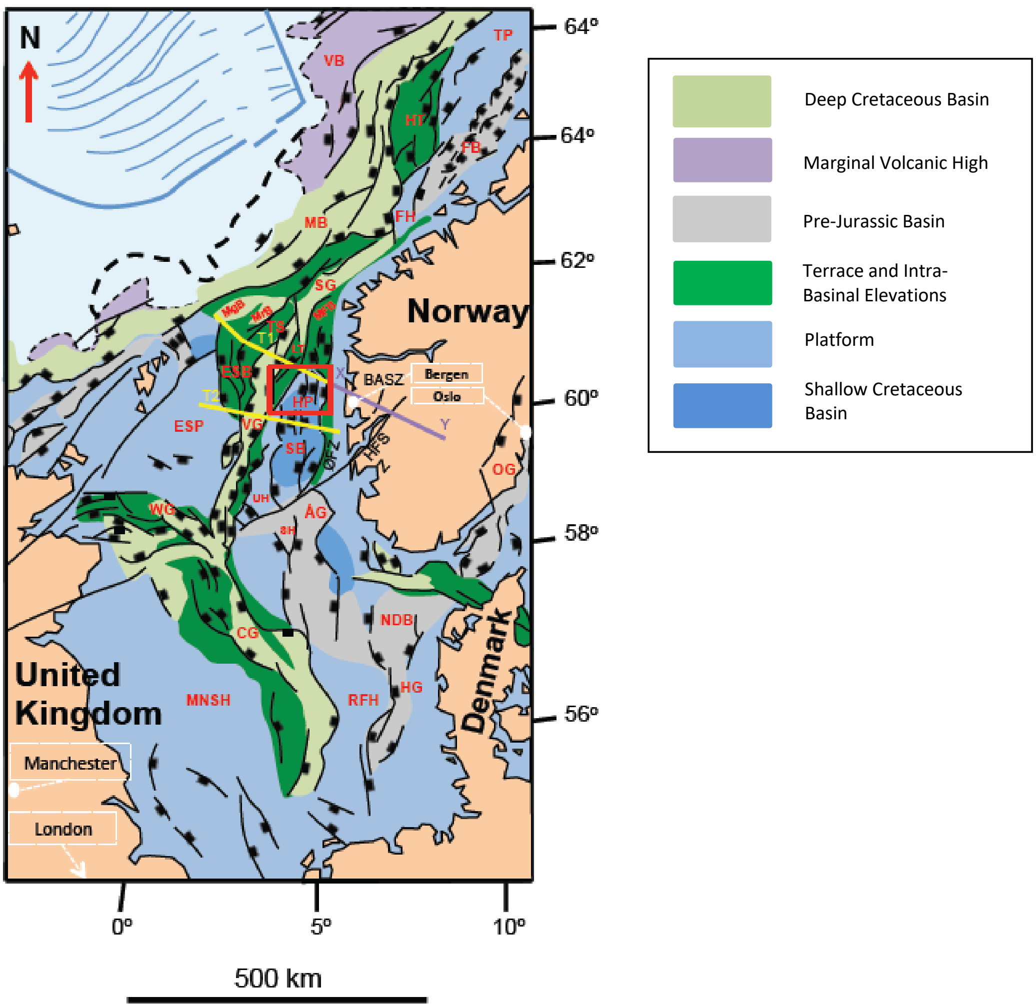

Figure 3-1: Map of the structural elements and basin distribution of the northern North Sea (Jonassen, 2015). Acronyms: CG-Central Graben, ESB-East Shetland Basin, ESP-East Shetland Platform, HG-Horn Graben, HP-Horda Platform, HT-Halten Terrace, MB-Møre Basin, MgBMagnus Basin, MNSH-Mid North Sea High, OG-Oslo Graben, SB-Stord Basin, SG-Sogn Graben, TS-Tampen Spur, UH-Utsira High, VG-Viking Graben, WG-Witchground Graben, ÅG-Åsta Graben (Jonassen, 2015).

Øygarden Fault Complex

The Øygarden Fault Complex (ØFC) is a regional structural lineament that marks the boundary between Horda Platform and western Norway crystalline massif and shows evidence of recent seismic activity (Bungum et al., 1991; Gabrielsen and Færseth, 1989). The ØFC extends for 300 km from Stavanger in the south to Florø in the north, running parallel to the western coast of mainland Norway with NNE-SSW strike. The fault complex has an intricate geological history, the details of which have been important for petroleum exploration in the North Sea. On the other hand, the offshore extent of the ØFC footwall is underexplored. The Øygarden Fault Complex is interpreted as one segment in the Permian-Triassic and three sub-segments in the Jurassic-Cretaceous. In that past few years, significant seismic activity has been observed on the northernmost segment of the ØFC, with e.g. a M3.7 earthquake in November 2017, felt by many inhabitants in the Bergen region (www.jordskjelv.no).

Nordfjord-Sogn detachment

The Nordfjord-Sogn detachment (NSD) separates the northern and central structural domains and coincides with the step-over region between the southern and northern segments of the Øygarden fault. The Nordfjord-Sogn detachment coincides with an abrupt change in seismic activity which suggests that this detachment plays an important role in the contemporary stress distribution offshore southwestern Norway. However, while contemporary seismicity delineates the Øygarden Fault Zone as an active structure, the mid-crustal depth distribution and small magnitude of the recorded events permits only a general correlation between the seismicity and surface faults.

3.2 Seismotectonic setting of the area

The seismotectonics of the North Sea, the Norwegian continental margin, and surrounding regions have been studied extensively since the mid 1970's, and especially after local seismic stations were installed in western Norway in the beginning of the 1980's. The most active research periods were during the 1980's and the 1990's because of the many large petroleum installations that required a seismic design, and this culminated in the national seismic zonation (NORSAR and NGI, 1998). However, during this time period the collection, collation and analysis of seismic data have continued steadily, and with increasing quality of both the network and the recorded data (resolution and bandwidth).

One of the first major seismotectonic studies for onshore and offshore Norway was carried out by Bungum et al. (1991), who summarized available seismicity and focal mechanism data at that time, concluding that the 'ridge push' force is a major source of stress, consistent with a NW-SE stress direction and dominantly reverse faulting along the continental margin.

A study that covers the seismotectonics of the present study region is by Møllegaard (2000). The starting point of Møllegaard was the availability of some high-resolution crustal transects in the North Sea, two of which are shown in Figure 3-2 and Figure 3-3. These transects, NSP-84-1 and NSP-84-2, cut through the northern and southern part of the study region, respectively, and as such they illustrate quite well the span of tectonic conditions in the study region. Møllegaard (2000) also reviewed in detail all available earthquake focal mechanisms. The solutions are mainly of mixed mode, indicating a complexity of the stress field at regional and local scales, together with a heavily fractured crust (especially around 61°N where also the number of mapped faults is very high). The study also clearly identified the Horda Platform as an aseismic region separating the Viking Graben, with indications of extension and normal faulting (Havskov and Bungum, 1987), from the coastal areas to the east and the complex areas north of 61°N where the two zones are merged. Continued monitoring of the seismicity however shows that a steady activity of small earthquakes is present, also on the Horda Platform. The main feature in the area is the Øygarden Fault.

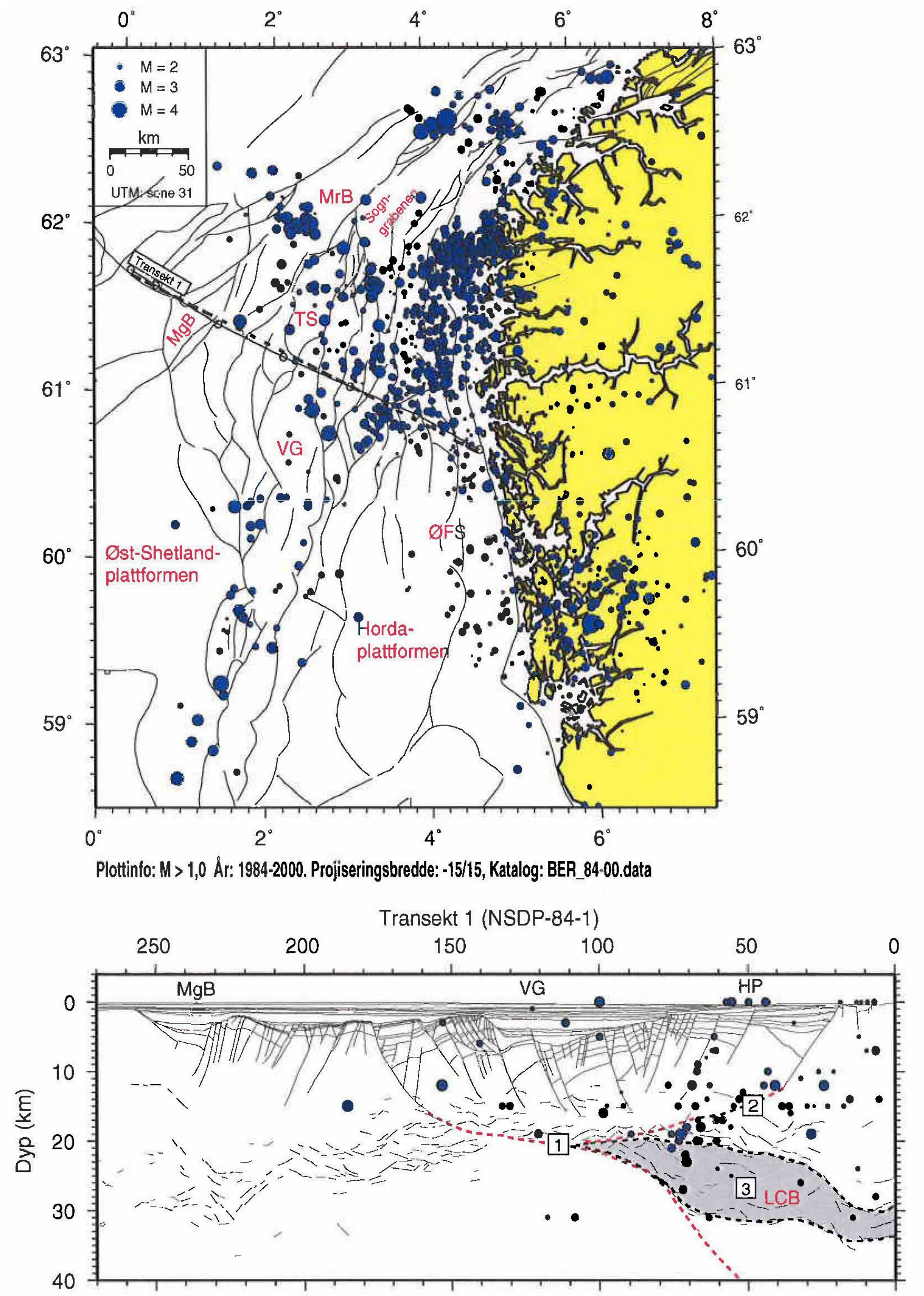

Figure 3-2: Earthquake distribution along profile NSP-84-1, projecting events (for the lower part of the figure) from 15 km on both sides of the line. Line 1 indicates the continuation of a basement fault down to an old shear zone, line 2 indicates the continuation of the Øygarden Fault Zone terminating on top of a lower crustal body (LCB, indicated by 3) (Møllegaard, 2000).

The northern transect (Figure 3-2) cuts through a seismically quite active area and the earthquakes occur rather deep and terminate at the top of the (high velocity) lower crustal body (LCB) as expected. At the eastern end of the transect, there is the connection to the Øygarden fault. The seismicity is significantly higher north of the Norway-Sogn detachment zone at 61°N, where also the displacements on the Øygarden fault are much more pronounced.

Around the southern transect (Figure 3-3), the seismicity is significantly lower and even more inconclusive, except that the hypocenters seem to be rather deep here as well. The twenty years of seismicity data, which now are available since Møllegaard performed his study, should provide a good basis for the analysis and discussions in the subsequent sections.

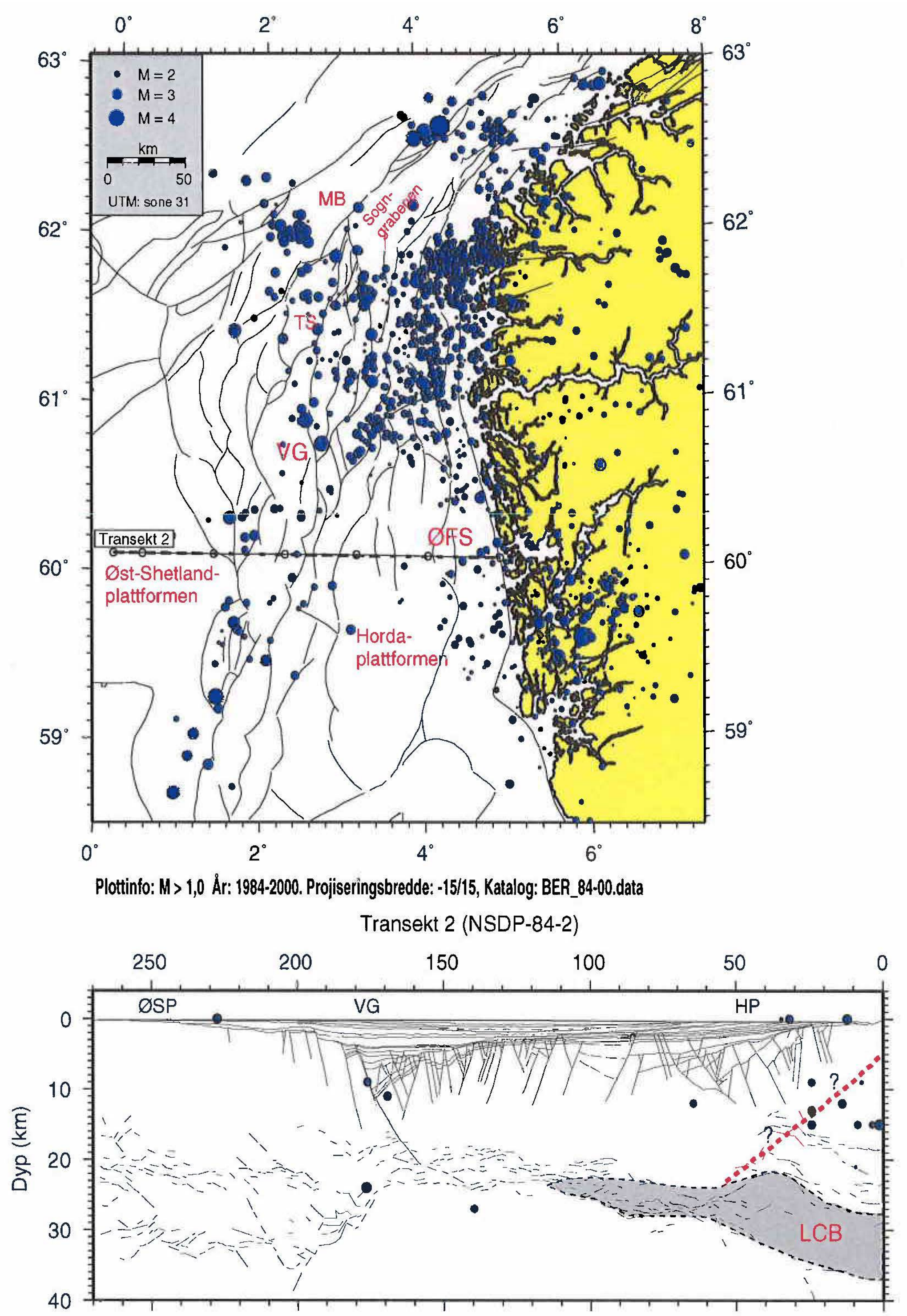

Figure 3-3: Earthquake distribution along profile NSP-84-2, projecting events (for the lower part of the figure) from 15 km on both sides of the line (Møllegaard, 2000).

4 Data and seismic analysis

4.1 Source model

The hazard calculation for this work is performed using two types of sources: area sources based on the seismicity distribution and a finite fault model for the Øygarden Fault Zone. These sources have been thoroughly examined and are described in the following section.

4.1.1 The earthquake activity and the catalogue

The earthquake catalogue is used to build the spatiotemporal occurrence model that can be employed as input for the seismic hazard assessment, providing a prediction model for a certain number of expected events occurring in different source regions with varying levels of magnitude.

The Norwegian Seismic Hazard Earthquake Catalogue (hereafter referred to as the NORSAR catalogue) is used for the analysis and covers the period up to the end of February 2026. For historical events from 1497 to the end of 2018, the catalogue includes events reported by national and international agencies, which have been qualitatively checked by NORSAR (Lindholm et al., 2025).

For the period from 2019 to end-February 2026, the catalogue is based on events from the Norwegian National Seismic Network (NNSN), including occasional updates according to NORSAR solutions. This most recent part of the catalogue is still under review and may be subject to further refinements in the future.

In addition, for both parts of the catalogue, all magnitudes are converted to a common scale, the moment magnitude scale (Mw). The moment magnitude is the standard magnitude scale required for the modelling of ground motion.

Recording and location of seismic events is conducted by the Norwegian National Seismic Network (NNSN). Their bulletins are based on data from seismic stations placed geographically throughout Norway. The stations are operated by the University of Bergen (UiB) and NORSAR, and the NNSN publishes monthly bulletins comprising location and magnitudes of the observed seismic events. Inevitably, explosions from mining, road and other construction sites may be mistaken for seismic events, and these man-made events may contaminate parts of the catalogue. The catalogue used for the present analysis was therefore processed further to remove such man-made events. The resulting catalogue is employed for quantitative analysis. However, the identification of explosions versus earthquakes is not failproof for smaller events on the mainland. Thus, only events with magnitudes exceeding 2.5 are used in the quantification process. The inclusion of explosions above this magnitude threshold cannot be excluded.

The distribution of regional seismicity within the NORSAR catalogue is shown in Figure 4-1 and Figure 4-2. Figure 4-1 shows the distribution of earthquakes in and around south-mid Norway as well as the area selected around the study region. The earthquake activity is highest west of Sognefjorden and extends southwards along the Viking Graben as well as along the coast of western and southwest Norway. A zoom of the area around the target region is shown in

Figure 4-2, which demonstrates that the seismic activity is higher north of the site than to the south of it. Figure 4-2 shows all earthquakes around the target region until end-February 2026 with magnitudes greater than or equal to 3.

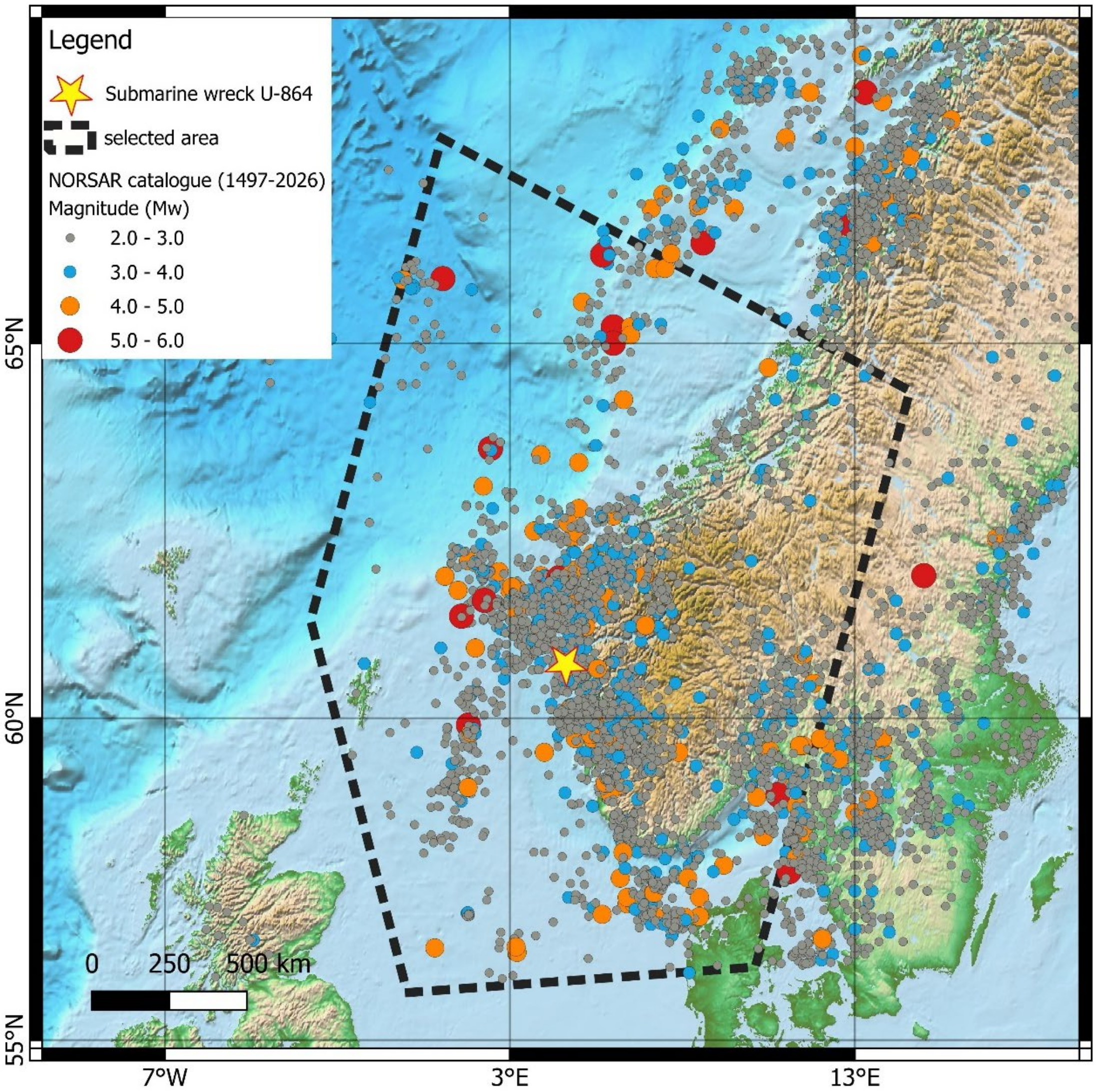

Figure 4-1: Earthquakes contained in the NORSAR catalogue with magnitudes greater than 2 in south-mid Norway. The submarine wreck U-864 location is indicated by the yellow star. The dotted black line confines region employed for earthquake statistics (section 4.1.1.3).

The largest earthquakes in and around southwestern Norway are listed in Table 4-1 and shown in Figure 4-3. The 1904 earthquake occurred in the outer Oslofjord region and was the cause for installing the first seismograph in Norway. The 1904 and 1927 earthquakes were located within the graben structures of the Oslo Graben and the Viking Graben, which all represent aborted rift structures from the Permian period. The location of the 1834 event in the Hardangervidda is very uncertain, especially because there is no recent significant earthquake activity within this region. However, the location is based on carefully analysed macroseismic data obtained from newspapers and other documentation.

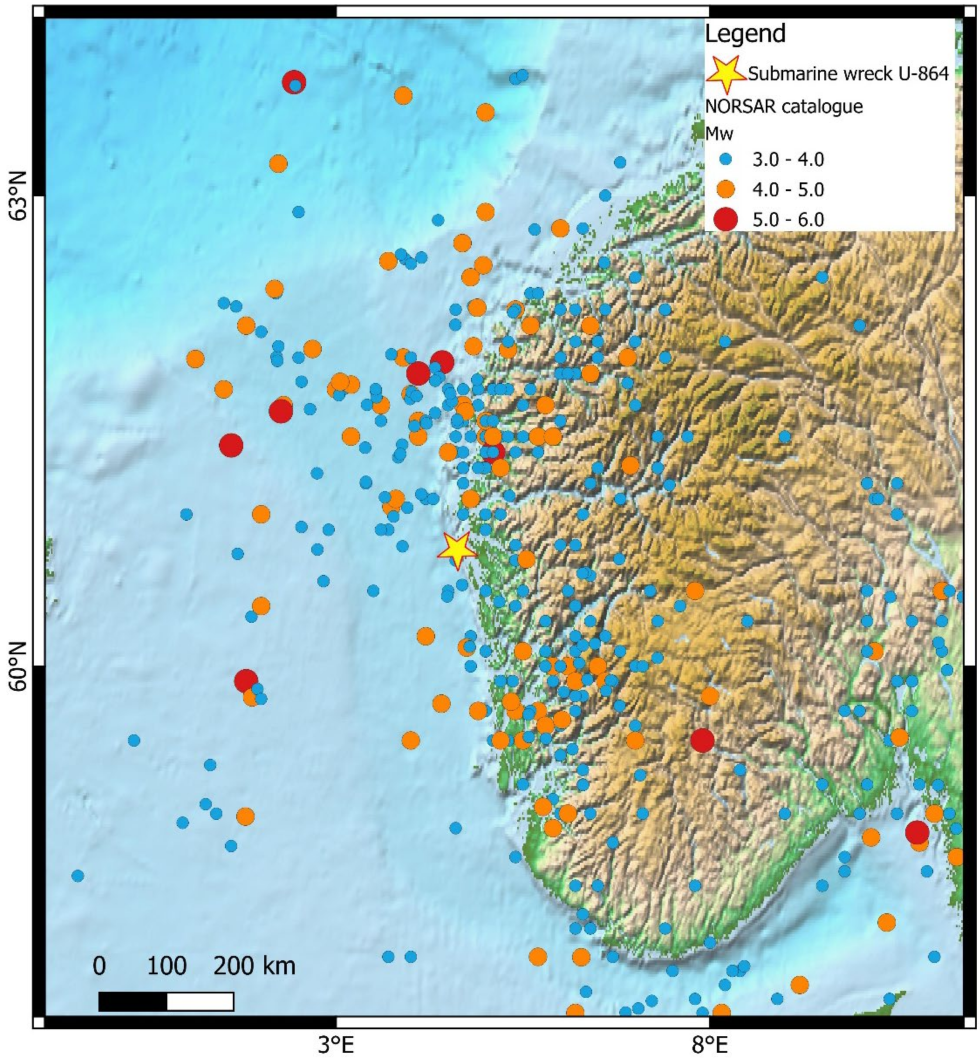

Figure 4-2: Earthquakes contained in the NORSAR catalogue with magnitudes greater than 3 up to end-February 2026. The submarine wreck U-864 location is indicated by the yellow star.

Table 4-1: Earthquakes within the study area with magnitudes estimated to be larger or equal to 5.

Date	Time	Lat	Lon	Depth (km)	Mw
03/09/1834	19:00:00	59.5	7.9	15	5
15/05/1892	14:51:00	61.4	5.1	15	5.2
23/10/1904	10:26:00	58.87	10.77	29	5.4
24/01/1927	05:18:00	59.9	1.8	15	5.2
03/06/1955	11:39:35	61.9	4.1	15	5.2
08/08/1988	19:59:32	63.68	2.44	25	5.3
17/09/1988	09:49:49	61.444	1.599	45	5.2
23/01/1989	14:06:29	61.97	4.42	26	5.2
21/03/2022	05:32:57	61.661	2.264	22.1	5.1

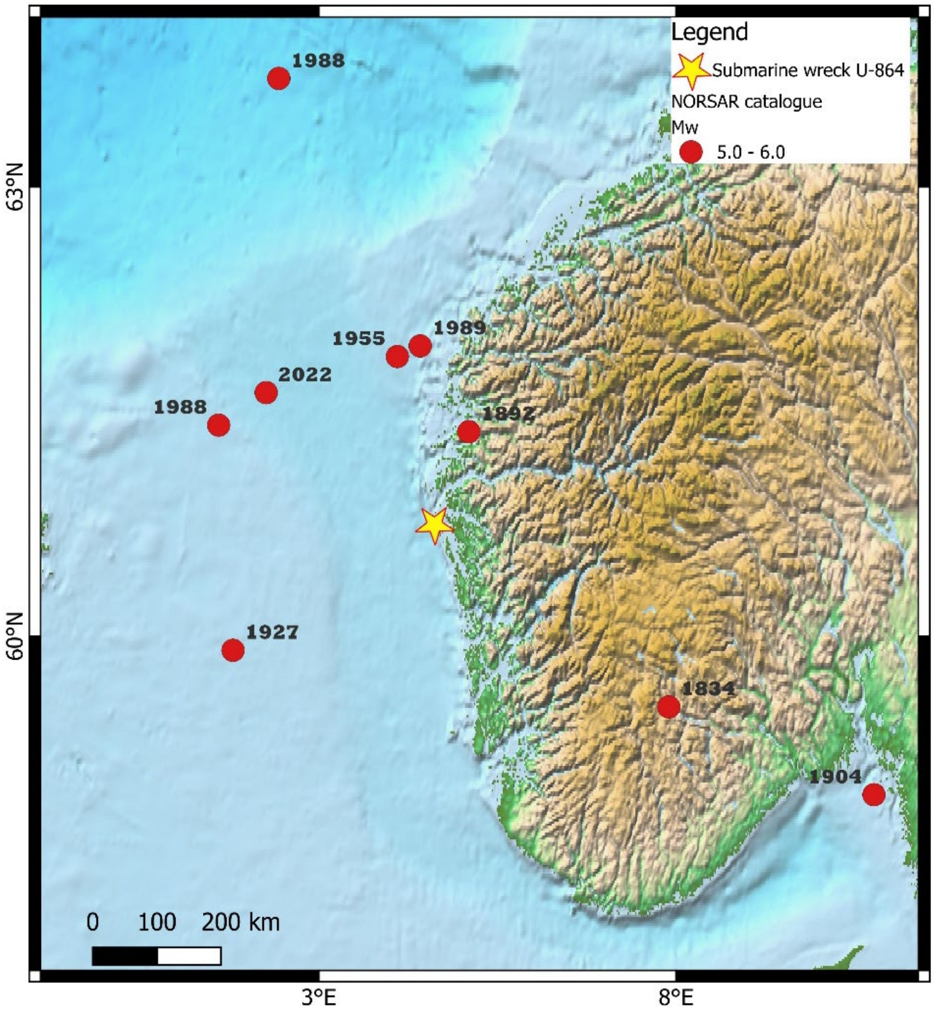

Figure 4-3: The largest earthquakes recorded in southwestern Norway based on revised source parameters. The submarine wreck U-864 location is indicated by the yellow star.

4.1.1.1 Catalogue declustering and completeness analysis

To justify the assumption of a Poissonian distribution of seismicity, declustering was applied to remove dependent events such as aftershocks and foreshocks, which can bias the recurrence parameters. Grünthal (Van Stiphout et al., 2012) method, designed for low-to-moderate seismicity regions, was selected. Starting from a dataset of 9,775 events within the selected area (Figure 4-1), the declustering process resulted in a refined catalogue of 9,169 independent events.

The magnitude of completeness (*Mc*) is the lowest magnitude above which all events in a specific space-time volume are detected. The magnitude of completeness of an earthquake catalogue is a value that affects the assessment of recurrence parameters, and thus, its estimation is a basic step for the processing of input data for seismic hazard analysis.

A manual procedure was carried out to characterise *Mc* based on the analysis of the obtained rates. Various tests, setting different thresholds for the calculation, were performed to understand the sensitivity of the magnitude of completeness. Finally, three values were considered for the calculation, resulting in 549 events employed for the PSHA analysis (Figure 4-4). We consider the catalogue to be complete for events with M ≥ 4 since 1880, for events with M ≥ 2.6 after 1980, and with M ≥ 2 in recent years. The inclusion of events from 2019 onwards that were not included in previous studies (Lindholm et al., 2025; NORSAR, 2019) clearly enhances the robustness of the dataset for recent low-magnitude seismicity. For events with M < 2, event recordings are distributed irregularly, primarily due to limitations in the sensor network's ability to detect and locate smaller events.

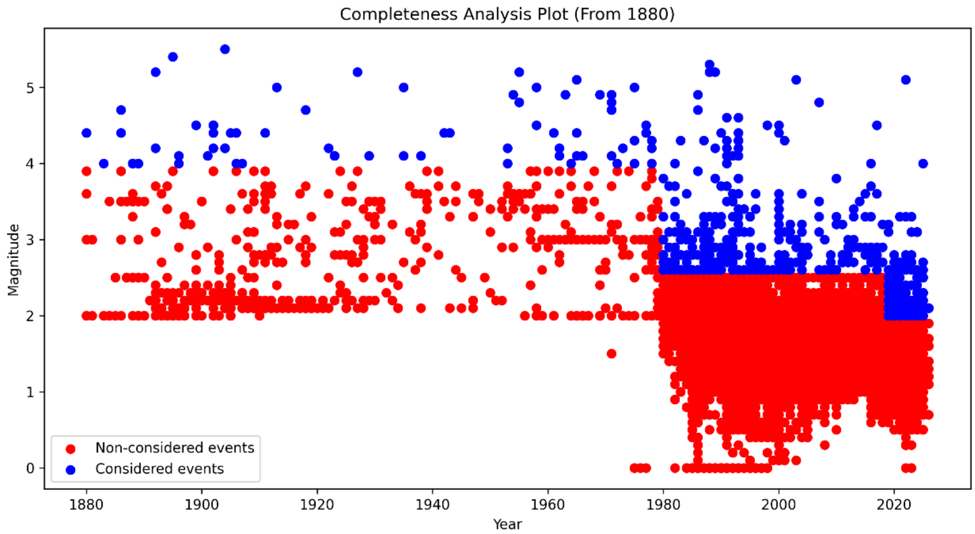

Figure 4-4: Time-magnitude plot for the identification of magnitude completeness thresholds.

4.1.1.2 The seismic zonation

The zonation has the purpose of dividing the area of investigation into distinct source zones and subsequently evaluating the seismic potential in each zone based on past seismicity. The area sources within each zone can be described as regions that have uniform source properties in time and space.

The main principle applied is to represent seismicity and tectonic structures as balanced as possible. Based on the tectonic knowledge, structural geology and earthquake catalogue, we divided the area following these principles:

- Each zone should be sufficiently large to allow for a statistically stable assessment of recurrence parameters, which requires an adequate number of events within each zone.
- A homogeneous source zone should encompass regions of uniform seismic potential and seismotectonic characteristics.
- The zones should cover all areas in which the seismicity could have an influence on the seismic hazard at the site of interest, which is usually ensured by including areas within 200-300 km distance, depending on the seismic activity level.
- The zonation should allow for regional differences in seismogenic conditions: e.g., focal depths, maximum magnitudes, and faulting mechanisms.
- The zonation should be consistent with the regional geology and tectonics.

We divided the area of investigation into eleven seismic zones (Figure 4-5) considering earthquake distribution, major faults, focal mechanisms, and the geological framework. The previously applied zonation model was also tested and resulted in very similar hazard estimates. Therefore, the updated zonation was selected, as it better reflects the distribution of the most recent seismicity and incorporates experience gained from other recent projects (NORSAR, 2025, 2022).

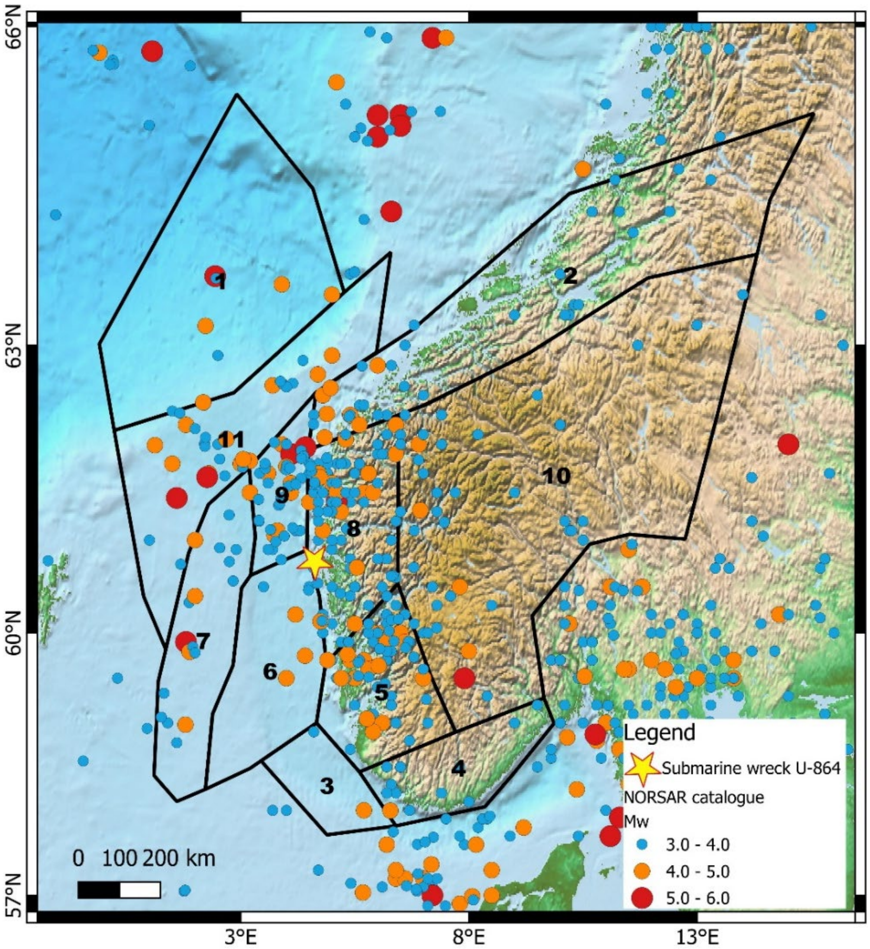

Figure 4-5: The updated zonation used in the computational model.

4.1.1.3 Quantification of earthquake recurrence

The distribution of earthquake magnitudes versus their frequency of occurrence is commonly found to follow a log-linear trend called the Gutenberg-Richter distribution (Gutenberg and Richter, 1956). The Gutenberg-Richter relationship implies a log-linearity in which $\log \boldsymbol{\lambda_m} = a - bm$ ($\boldsymbol{\lambda_m}$ is the number of earthquakes equal to or larger than magnitude m, a and b are regression coefficients). The b-value (the slope of the distribution) represents the scaling value between larger and smaller magnitude earthquakes. Globally, it is found to be close to 1, whereas the a-value (y-axis intercept) varies from region to region, reflecting the level of seismic activity. These parameters must be estimated with care, requiring a sufficiently large and representative dataset to ensure statistically stable and meaningful results, as they have a direct impact on the resulting seismic hazard.

Because the b-value is expected to be related to the large-scale seismotectonic regime, we assume the b-value to be stable within our regional study area, both with time and space, even though local studies sometimes observe minor differences. The determination of the b-value requires many events to be statistically valid, we computed a single, regional b-value for the whole study region framed by the dotted line in Figure 4-1.

To assess its stability, the b-value was calculated by two different methods, namely linear regression (Gutenberg and Richter, 1956) and maximum likelihood method (Bender, 1983). Results from both methods are presented in Figure 4-6 and yield b-values from 0.85 to 1.15, depending on method and completeness period. While both methods produce consistent estimates, we assign more weight to the results from the maximum likelihood method due to its stronger statistical foundation and lower sensitivity to binning effects. Based on this approach, we adopt a representative b-value of 0.90 (corresponding to β-value of 2.0809 with $\beta = \mathrm{b} \cdot \ln 10$) for the entire region. For the maximum likelihood method, the analysis was performed separately for each completeness period, and the corresponding b-values are shown in distinct plots. For the linear regression, although the analysis likewise accounted for the three completeness periods, the results are presented in a single consolidated plot.

The λ-value for each zone represents the number of earthquakes normalised by observational period, therefore representing the annual occurrence. The λ-values were migrated to a magnitude threshold of 4.5, using the previously obtained b-value. The model parameters for each zone are provided in Table 4-2. Events with a magnitude of less than 4.5 are considered to be of limited engineering significance.

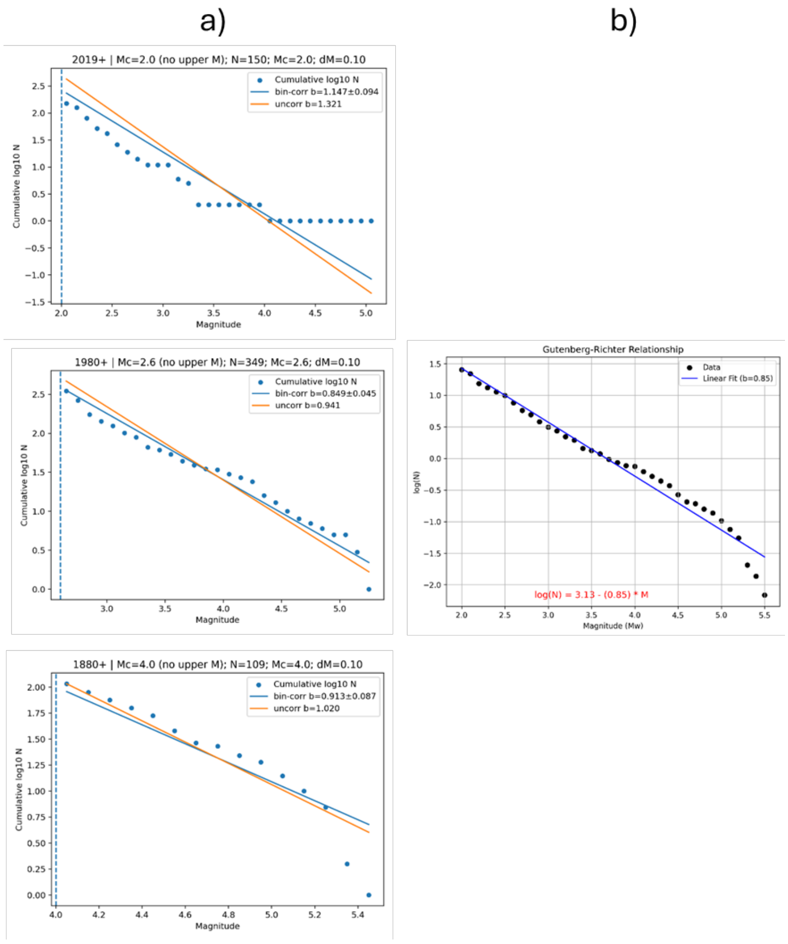

Figure 4-6: b-value computation for the whole study region shown in Figure 4-1. a) Results obtained using the maximum likelihood method, shown for the three completeness periods separately. b) Results obtained using linear regression, considering the same three completeness periods, presented in a single consolidated plot.

Table 4-2: λ-values obtained for the 11 zones as used in the computational model and constant *β*-value based on b-value of 0.9).

Zone	*β*-value	λ-value for M=4.5	Return period (yr) for M=4.5
1	2.0809	0.005410	185
2	2.0809	0.010075	99
3	2.0809	0.000304	3287
4	2.0809	0.001391	719
5	2.0809	0.017915	56
6	2.0809	0.003658	273
7	2.0809	0.013281	75
8	2.0809	0.021539	46
9	2.0809	0.023617	42
10	2.0809	0.006357	157
11	2.0809	0.024167	41

4.1.1.4 Maximum magnitude calibration

The estimation of the maximum magnitude (M_{max}) to be used in the seismic hazard analysis is a complex process guided by information from geology and seismotectonics of the investigated seismic region. In this study, we applied Mmax = 6 as the maximum magnitude with an assigned uncertainty of ±0.3 for all area sources.

Since the final PSHA model includes both area sources and a fault model, the value of M_{max} is used to distinguish between the seismic potential of both source types. Basically, for magnitudes lower than 6, the seismic potential is attributed to the area sources, while for magnitudes greater than 6, the seismic potential is related to the fault model (in this case, the Øygarden Fault Zone).

4.1.1.5 Focal depth distribution

Earthquake focal depth is of vital importance for hazard assessment, since an increasing source distance (including source depth) reduces the shaking intensity. The earthquake focal depth is usually more uncertain than its geographical (epicentre) location, and the uncertainty increases with decreasing earthquake magnitudes. In Norway, the earthquake activity is dominated by small magnitude earthquakes, often located offshore. In this case, source-station distances are significant and azimuthal gaps are large, creating large uncertainties.

We know from earlier studies (Bungum et al., 1991; Hicks et al., 2000) that focal depths for earthquakes in Norway are distributed throughout the entire crust, but with significant variations depending on sub-region. The results obtained from Lindholm et al. (2000) for onshore and offshore southwestern Norway demonstrate a clear tendency of coastline earthquakes to be located at shallower depths and of offshore events to be situated at larger depths. This tendency was also observed in the NEONOR2 project covering seismicity in Nordland (Olesen et al., 2018).

Lindholm et al. (2005) demonstrated that onshore earthquakes in coastal areas occur primarily in the upper crust (less than 15 km depth) with a tendency for normal faulting, while offshore earthquakes are more commonly found in the lower crust, where reverse faulting is more prevalent. As general earthquake source depth in the zonation, we use 12 km depth for onshore areas and 15 km depth for offshore areas, well noting, that the uncertainties of both source depths are about 5-10 km, depending on earthquake size and distance to recording seismic stations.

Within the study area (see Figure 4-1), the focal depth distribution of events included in the analysis is reported in Figure 4-7 showing that most earthquakes occur at depths between 15 and 20 km, but fraught with large uncertainties.

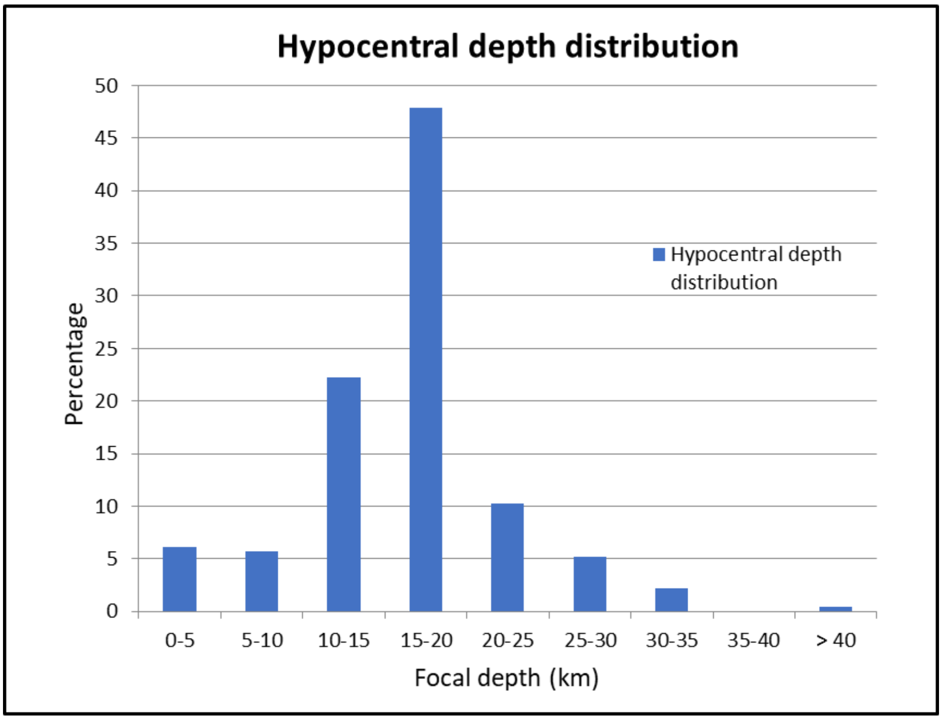

Figure 4-7: Focal depth distribution of all earthquakes within the area shown in Figure 4-1.

4.1.1.6 Catalogue uncertainties

Many uncertainties affect the earthquake catalogue. These uncertainties are related to the magnitude estimation, the epicentral locations, and the depths of the events. Another source of uncertainty is linked to the short observation period in comparison with the recurrence times of large earthquakes. For example, the observation period of earthquake activity in Norway covers only about 130 years, including newspapers and other written documentation. Since the expected return period of large earthquakes is much longer than 130 years, the uncertainty of any hazard estimate is significant. Even though we are using a catalogue that is as complete and as reliable as possible, we have to rely on additional information from geological and seismotectonic observations to adjust the parameters for long return period estimates. These adjustments are based on expert judgment and are also a source of uncertainty.

4.1.2 Faults

In seismic hazard assessment, known geological structures are explicitly incorporated as discrete faults, assigning seismic potential to specific mapped faults based on their geometry, slip rate, and recurrence intervals. This method provides a more deterministic view of seismic hazard but relies on well-constrained fault activity data. However, such data is lacking for most faults in the study area, which show no clear signs of recent movement.

Among the identified structures, only the Øygarden Fault Zone has a large-scale reactivation potential, and it is therefore included in the final PSHA model alongside the distribution of past seismicity in the area. Other mapped major structures have been exclusively used to define the seismic zonation.

4.1.2.1 Segmentation

Fault zones are rarely uniform, they often exhibit geometric complexities like bends, steps, splays, and branches. Different fault segments may have different mechanical properties or behaviors, influencing rupture characteristics, such that seismicity parameters such as slip rate, maximum magnitude (Mmax), and recurrence interval may vary significantly along the fault. Ruptures often do not span an entire fault zone, especially if separated by physical or structural barriers; even entire fault segments may act as rupture barriers or asperities. Subdividing the fault into segments allows to capture variations in fault properties and behaviour and enables to model partial or segment-limited ruptures, which are more realistic and frequent than full-fault ruptures, improving ground motion estimations for nearby sites. The segmentation of the Øygarden Fault Zone reflects the fault's natural structure and behaviour. It accounts for bends, discontinuities, and variations along the fault, and allows for more realistic estimates of recurrence and rupture extent. Although we cannot completely exclude the possibility of a fault rupturing in a single large event, we consider such scenarios to have extremely low probability based on the regional tectonic setting and the current seismic activity in Norway. Higher magnitude scenarios resulting from earthquakes breaking a longer segment of the fault are accounted for through the epistemic uncertainty expressed in the maximum magnitude range.

The Øygarden Fault Zone extends from Stavanger in the south to Florø in the north running parallel to the western coast of mainland Norway. It is a normal fault with NNE-SSW strike, dipping 70° to the west. Figure 4-8 highlights that the Øygarden Fault Zone is divided into three principal segments with lengths of 175 km, 115 km and 85 km, respectively, from south to north. In order to account for typical fault characteristics, the three parts were subdivided further. After an in-depth literature review (Bell et al., 2014; Faleide et al., 2015; Ramberg et al., 2007; Smirnova, 2019), adequate fault width values were extracted to compute the aspect ratio (i.e., the fault length/fault width factor), which is a key input for determining maximum magnitude. Figure 4-9 shows a graphical overview of fault source parameters, and details of the segmented fault model are provided in Table 4-3.

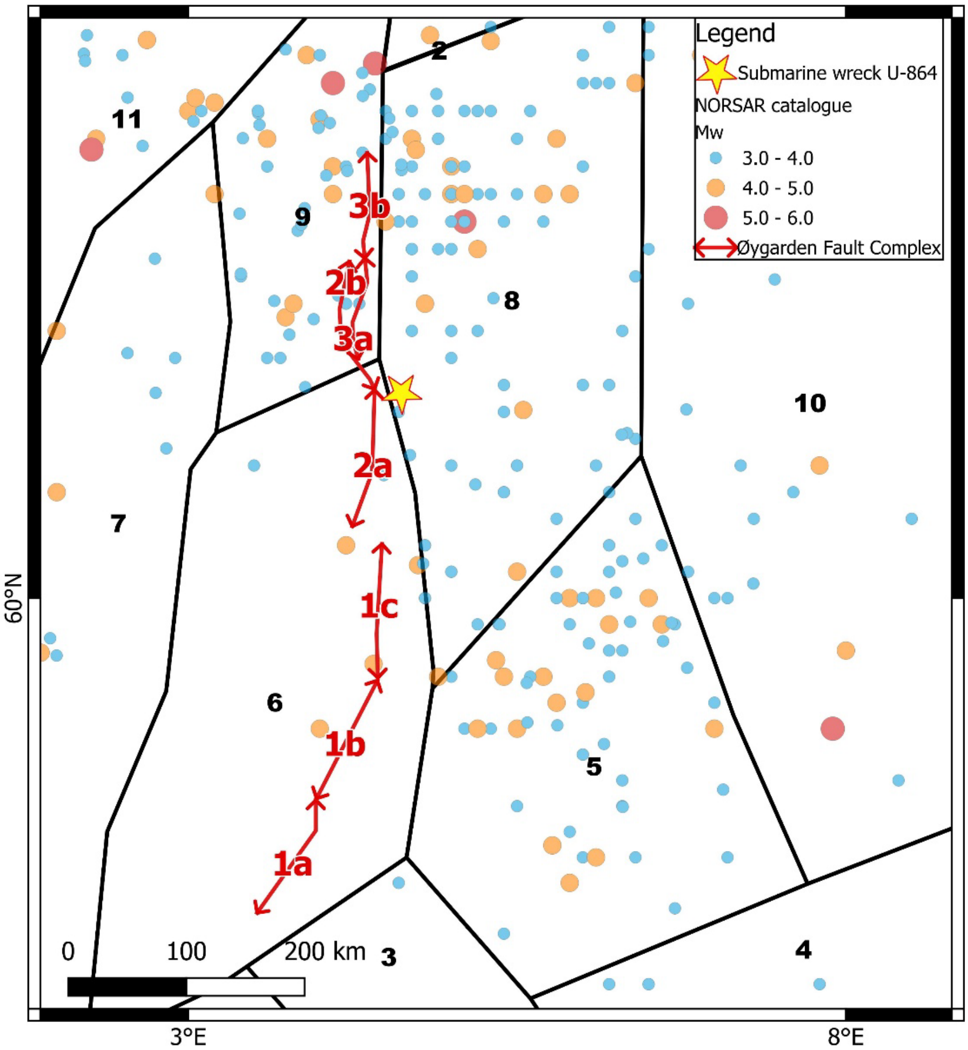

Figure 4-8: Segmentation of the Øygarden Fault Zone. Numbers represent the three principal segments of the Øygarden Fault Complex considered in this study, while letters denote the subdivision of the principal segments into sub-segments. The NORSAR catalogue and the seismic zones are also shown.

Table 4-3: Summary of the Øygarden fault segments (assumed as rectangular fault planes), dip angles, widths, lengths, the length of each sub-segment, and the aspect ratios of the sub-segments.

Fault	Dip angle (◦)	Width (km)	Original length (km)	Number of segments	Length of sub-segments (km)	Aspect ratio
Øygarden 1	70	29	175	3	58	2.0
Øygarden 2	70	26	115	2	57.5	2.2
Øygarden 3	70	26	85	2	42.5	1.6

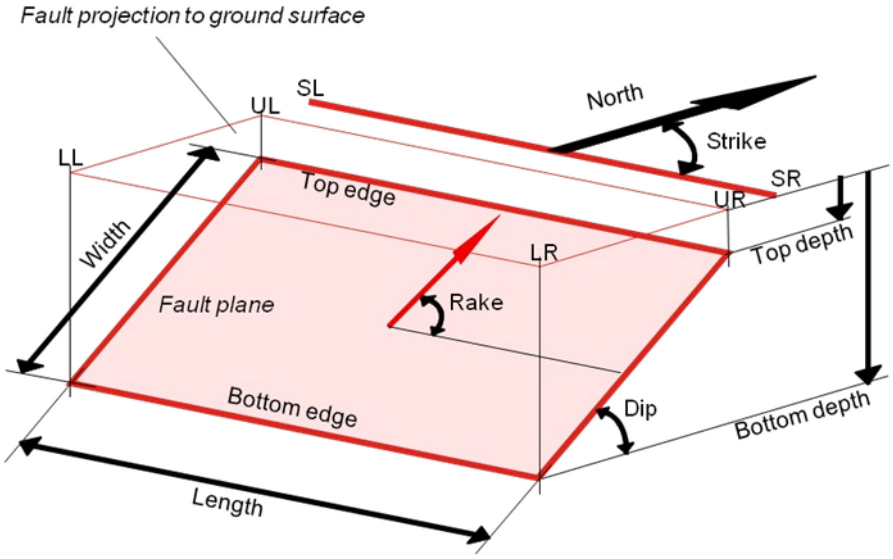

Figure 4-9: The fault surface is obtained by translating the fault trace from the Earth's surface to the lower seismogenic depth (bottom depth) with an inclination equal to the dip angle. The upper seismogenic depth delimits the fault top edge. A mesh representation of the fault plane is then constructed. The figure also shows the width and the length of a fault seismogenic source.

4.1.2.2 Recurrence parameters and maximum magnitude

To extract the recurrence parameters, it is important to quantify the seismic activity level of the fault. Based on Bell et al. (2014), different values of slip rates were associated to the segments of the Øygarden Fault Zone, including temporal changes. Bell et al. (2014) estimated these slip rates by measuring the fault's vertical displacement (throw) across dated stratigraphic horizons using seismic reflection data and then dividing the throw by fault dip and the duration of activity to derive average slip rates. The slip rate values range from 0.02 to 0.3 mm/yr. We decided to apply a conservative value of 0.3 mm/yr in the final model as worst-case scenario.

Knowing the slip rate (S) and the rupture length of the Øygarden Fault Zone (Bell et al., 2014; Smirnova, 2019), we extract values for λ and Mmax (Bungum, 2007), employing the model developed by Youngs and Coppersmith (1985):

$$\lambda(\mathrm{m}^0) = \frac{\mu A_f S(d-b)[1-e^{-\beta(m^u-m^0)}]}{bM_0^u e^{-\beta(m^u-m^0)}} \quad (3)$$

where m^0 is an arbitrary reference magnitude, μ is the shear modulus, $A_f = LW$ is the fault area, S is the slip rate, d is the average displacement per event $\beta = \mathrm{b} \cdot \ln 10$, m^u is an upper bound magnitude and M_o^u is the seismic moment associated with m^u.

The calculation was performed for m^0= 6, the magnitude value that was chosen as the upper limit for the area sources and the lower limit for the fault sources. In addition, the *b*-value was fixed to 0.9037, similar to the area sources, corresponding to a β-value of 2.0809. All values area listed in Table 4-4.

Table 4-4: Slip rate, recurrence parameters, minimum and maximum magnitude used in the hazard model as well as return period for a M=6 event for the Øygarden fault.

Fault	Slip rate (mm/yr)	β-value	λ-value (for M=6.0)	M_{min}	M_{max}	Return period (yr) for M=6.0
Øygarden 1	0.3	2.0809	0.001287	6.0	7.4	777
Øygarden 2	0.3	2.0809	0.001224	6.0	7.3	817
Øygarden 3	0.3	2.0809	0.001072	6.0	7.2	933

It is important to mention that the evaluation of M_{max} is not a simple procedure and is affected by uncertainties. The common approach for area sources in stable and active continental regions is to define M_{max} through a combination of the observed maximum magnitude for each zone and the evaluated tectonic potential. A simple, yet commonly applied rule is that M_{max} should be set to about 0.5 magnitude units above the largest observed value. The tectonic potential depends strongly on the existence of faults. Often, the total length of a fault is considered, however, the maximum magnitude depends on the size of the fault patch that slips in a single event, and the magnitude is higher the larger the fault patch is. Therefore, in this study, M_{max} is estimated based on the length of each fault sub-segment. To calibrate the combined hazard model, we use the M_{max} values for the Øygarden Fault Zone as listed in Table 4-4 including uncertainties of ±0.3.

4.1.2.3 Fault uncertainties

Fault uncertainties are related to the location and geometry of the fault traces, the slip rates as well as their dip and width. These uncertainties are even larger in low seismicity regions like Norway. Onshore, these uncertainties arise from limited surface expressions, erosion, and sediment cover that obscure fault traces, making field observations and morphological analysis more difficult. Offshore, uncertainties are also due to the resolution limits of seismic imaging, sedimentation processes that mask fault activity, and difficulties in dating marine deposits to estimate slip rates.

One way to overcome the problem is to account for potential variations in the fault geometry (strike, dip and depth) and by weighting them differently in the model. Estimates of the slip rates are usually afflicted with high uncertainty and often, some parts of the slip will be accommodated by future earthquakes. To build a credible model, the change in recurrence parameters assuming different slip rates should be analysed to ensure their balance. While acknowledging all these uncertainties, in the current model we capture epistemic uncertainty using uncertainties of ±0.3 for M_{max} and ±0.25 for the β-value (corresponding to ±0.1 for the b-value). After performing a sensitivity analysis of different slip rate values, we decided to adopt a conservative value to represent a worst-case scenario.

4.2 Ground Motion Prediction Equations

Ground Motion Prediction Equations (GMPEs), also referred to as ground-motion models (GMMs), describe the expected distribution of ground-motion intensity measures as a function of earthquake magnitude, distance, and site conditions. They therefore represent a critical component of probabilistic seismic hazard analysis. Because no GMPEs have been specifically developed for Norwegian seismic conditions, hazard studies in the region typically rely on models developed for tectonic environments considered broadly comparable, such as stable continental regions and shallow active crustal regions.

In the 2019 seismic hazard study for the U-864 site, the earthquake loading analysis was performed using three GMPEs within a logic-tree framework: (Atkinson and Boore, 2006; Bindi et al., 2011; Cauzzi et al., 2015). These models were selected to represent both active shallow crustal and stable continental region conditions considered relevant for the Norwegian margin.

Since then, additional ground-motion models and improved datasets have become available. A comprehensive evaluation of candidate GMPEs for Norwegian offshore conditions was recently conducted in a separate study (NORSAR, 2025). That work assessed a suite of candidate models through scenario-based comparisons and goodness-of-fit analyses against available North Sea ground-motion data. Based on these analyses, eight GMPEs representing both active shallow crustal region (ASCR) and stable continental region (SCR) conditions were selected and combined in a weighted logic-tree framework.

Given the similar tectonic context and offshore location of the U-864 site, the results of the GMPE evaluation in NORSAR (2025) are considered applicable to the present study. Therefore, the same set of GMPEs and logic-tree weights are adopted here. This approach allows the updated hazard model to incorporate recent developments in ground-motion modelling while maintaining consistency with current best practice for seismic hazard studies in the Norwegian offshore region.

The PSHA computations are performed for reference rock conditions corresponding to Vs30 = 1200 m/s, which is consistent with the reference site conditions adopted in the recent studies (Lindholm et al., 2025; NORSAR, 2025, 2022) and represent stiff rock conditions appropriate for bedrock environments. Hazard results therefore correspond to bedrock ground motions, allowing direct comparison with the 2019 results. The selected GMPEs are briefly described below.

1. Weatherill and Cotton (2020): A backbone model developed for the stable cratonic regions of Europe as part of the ESHM20 hazard model. It represents updated modelling of ground motions in low-seismicity continental regions.
2. kkar et al. (2014): Empirical ground-motion model derived primarily from the European RESORCE strong-motion database for active shallow crustal regions. The model is widely used in European hazard studies and performs well across a broad range of magnitudes and distances.

3. Bindi et al. (2017): Empirical model calibrated to European conditions using a combination of NGA-West2 relations and regional data. It provides stable magnitude scaling and is suitable for moderate-magnitude events typical of intraplate European seismicity.
4. Cauzzi et al. (2015): Global empirical GMPE based on both NGA-West2 and RESORCE databases. The model covers a broad period range and is commonly used in international hazard studies.
5. Yenier and Atkinson (2015): A stochastic model developed for stable continental regions using an equivalent point-source approach. It incorporates adjustments for regional stress drop and attenuation characteristics.
6. Boore (2015): A ground-motion model from the NGA-East project for stable continental regions, using the Atkinson and Boore (2014) model
7. Rietbrock and Edwards (2019): A stochastic GMPE developed for the United Kingdom based on regional earthquake data and simulations, representing stable continental crust conditions.
8. Pezeshk et al. (2018): A stochastic model based on the NGA-East database for stable continental regions, included to provide additional representation of epistemic uncertainty.

These models are combined with a logic-tree framework to represent epistemic uncertainty in ground-motion prediction. The GMPEs and their corresponding weights adopted from NORSAR (2025) are summarized in Table 4-5.

Table 4-5: Ground Motion Prediction Equations (GMPEs) applied in this study. “Region” denotes the province for which the model was developed (mEast = Middle East, CENA = Central and Eastern North America). “Data/Method” refers to the data base and the method used. “M range” and “R range” are the magnitude and distance range of applicability claimed by the authors. “Faulting style” is “All” if the relation is valid for all three types of regimes (strike slip, normal, and reverse), “U” if unspecified. “PSA range” is the period range for the pseudo-spectral acceleration (PSA). “Site cond. (Vs30)” provides the site conditions in terms of Vs30 “*” indicates that the reference rock side condition can be amplified using linear and nonlinear site amplification models (Hashash et al., 2020; Stewart et al., 2020). “Weight” indicates the logic-tree weights assigned to each model.

No	Reference	Short name	Tectonic Region /Type	Region	Data /Method	M range (mag)	R range (km)	Distance metric	Faulting style	PSA range (s)	Site cond. (Vs30 m/s)	Weight
1	Weatherill and Cotton (2020)	CG20	SCR / Backbone	Europe cratonic	NGA-East, Equiv. point source	3.5-8.0	0-500	rup	U	0.01-10	800*	0.22
2	Akkar et al. (2014a,b)	ASB14	ASCR / Empirical	Europe-mEast	RESORCE	4.0-7.6	0-200	jb, epi, hypo	All	0.01-4	150-1200	0.18
3	Bindi et al. (2017)	BCK17	ASCR / Empirical	Shallow crustal	NGA-West2	3.0-7.9	4-300	jb, hypo	U	0.02-4	360-1500	0.18
4	Cauzzi et al. (2014)	CFV15	ASCR / Empirical	Global	NGA-W2, RESORCE	4.5-7.9	0-150	rup	All	0.01-10	150-1200	0.18
5	Yenier and Atkinson (2015)	YA15	SCR / Stochastic	CENA	Equiv. point source	3-8	0-600	rup	U	0.01-10	150-1500	0.18
6	Boore (2015)	B15_AB14	SCR / Stochastic	CENA	NGA-East, Equiv. point source	4.0-8.0	0-1200	rup	U	0.01-10	3000*	0.02
7	Rietbrock and Edwards (2019)	RE19	SCR / Stochastic	UK	UK	3.0-7.0	0-300	Rjb	U	0.03-5	Rock	0.02
8	Pezeshk et al. (2018)	PEZ18	SCR / Stochastic	CENA	CENA	4.0–8.0	1–1000	Rrup	U	0.01-10	3000*	0.02

5 Results

All computations were conducted combining the area source model and the Øygarden Fault Zone model in a logic tree employing the 8 selected GMPEs with different weights. In the following, the input parameters for the computational model are listed:

Seismic sources: 3 fault sources (7 fault segments) and 11 area sources.

Return periods: 100, 475, and 10,000 years.

Results: Uniform Hazard Spectra (UHS) at bedrock for the submarine wreck U-864 location.

Structural periods for computation: 0.01 (PGA equivalent), 0.05, 0.1, 0.2, 0.5, 1.0, 1.5, 2.0 and 3.0 seconds.

GMPEs: as listed in Table 4-5 with different weights in the logic tree. GMPEs were used with a Vs_{30} of 1,200 m/s.

Lower bound magnitudes: M4.5 for all area sources, and M6.0 for all fault sources.

Upper bound magnitudes: M6.0 for all area sources, and M7.2-7.4 for fault sources.

Uncertainty of Mmax: 0.3

β **(regression-based):** 2.0809 ± 0.25.

λ **(counting-based):** as provided in Table 4-2 and Table 4-4.

Rupture extension parameters: generic from Wells and Coppersmith (1994).

Focal depths: 15 km for offshore area sources, 12 km for onshore area sources, as well as 13 and 14 km, respectively, for fault sources.

Global activity parameters used in the model: maximum integration distance: 300 km; maximum triangle size: 11 km; minimum distance/triangle size ratio: 7 km.

5.1 PSHA results at bedrock

5.1.1 Hazard curves

The effects of earthquakes of different magnitudes occurring at multiple locations belonging to various sources with varying probabilities of occurrence are integrated into the so-called hazard curve that shows the probability of exceeding different levels of seismic ground motion (such as Peak Ground Acceleration, PGA) at a site during a defined period of time.

In the following, the hazard curves for all considered frequencies are plotted exemplarily for a probability of exceedance of 50 years for the submarine wreck U-864 location (Figure 5-1).

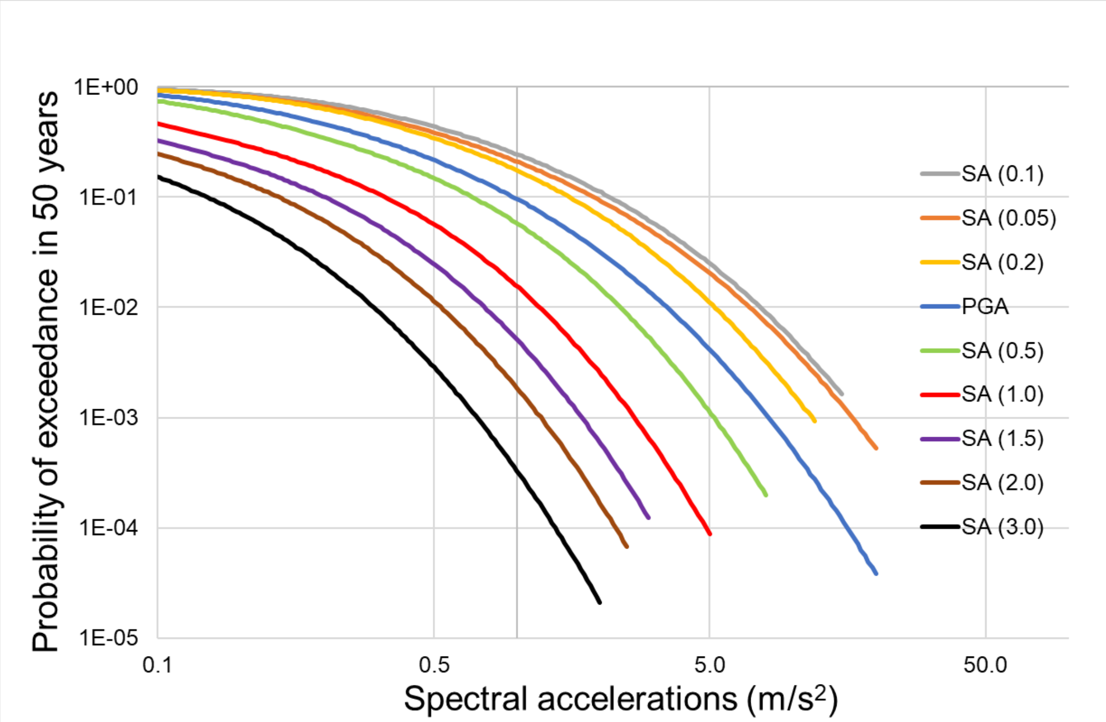

Figure 5-1: Hazard curves for a suite of spectral accelerations (in m/s^2) in terms of probability of exceedance in 50 years for the submarine wreck U-864 location.

5.1.2 Uniform Hazard Spectra

As opposed to the hazard curves, the Uniform Hazard Spectra (UHS) display the spectral acceleration for a range of periods with a uniform probability of exceedance. In this study, we provide the UHS for three return periods (100, 475, and 10,000 years) that correspond to the following probabilities of exceedance: 40% in 50 years, 10% in 50 years, and 0.5% in 50 years. The 475-year return period is used mainly for onshore structures, while 100- and 10,000-year return periods are employed for offshore structures. In Figure 5-2 the spectral acceleration (in cm/s^2) is plotted versus period for the submarine wreck U-864 location for the three return periods.

The updated UHS for the U-864 site are compared with the results from the 2019 study in Figure 5-2. Overall, the 2026 results show slightly higher spectral accelerations across most periods and return periods, with the most pronounced differences observed at short periods (high frequencies). The general shape of the spectra remains consistent with the 2019 results, since the underlying seismotectonic framework has not changed.

The numerical values corresponding to the UHS shown in Figure 5-2 are summarised in Table 5-1. The comparison confirms that the increase is most pronounced at short periods, while differences at longer periods are smaller and, in some cases, slightly lower than the 2019 results. This behaviour is consistent across all return periods and reflects the influence of the updated ground-motion models and revised seismicity parameters in the hazard analysis.

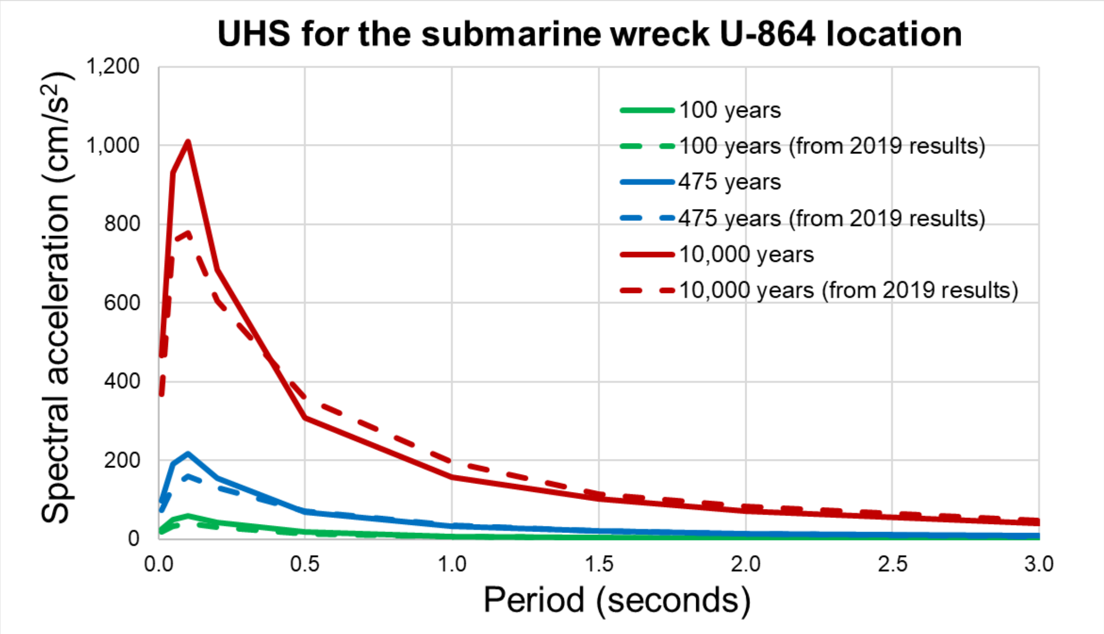

Figure 5-2: Uniform Hazard Spectra (UHS) for the U-864 location showing spectral acceleration (in cm/s²) versus period (in seconds) for return periods of 100, 475, and 10,000 years. Updated 2026 results (solid lines) are compared with the 2019 results (dashed lines).

Table 5-1: Comparison of spectral acceleration values (cm/s²) for the U-864 site for return periods of 100, 475, and 10,000 years, showing results from the 2019 study and the updated 2026 model.

	Spectral acceleration (cm/s²)					
	100 yr		475 yr		10,000 yr	
Period (s)	***2019***	***2026***	***2019***	***2026***	***2019***	***2026***
0.01 (PGA)	17	25.2	72	97.3	367	465
0.05	33	49	133	190	756	930
0.1	39	57.8	160	217	777	1010
0.2	31	42.4	130	155	605	684
0.5	14	16.8	70	69.1	358	309
1.0	6	6.63	35	33.2	195	158
1.5	3	3.57	20	20.1	115	101
2.0	2	2.25	14	13.7	82	70.3
3.0	1	1.14	7	7.54	46	40.5

6 Discussion and conclusions

The updated PSHA results for the U-864 site indicate a general increase in hazard levels compared to the 2019 study, particularly at short spectral periods. The most pronounced differences are observed for Peak Ground Acceleration (PGA) and short-period Spectral Acceleration (SA), with increases on the order of 40-50%, while differences at longer periods are smaller and generally within 10-20%.

These changes are primarily driven by the updated and new ground-motion prediction equations (GMPE) that are included in the logic tree computations, which now include eight models instead of three. The inclusion of additional GMPEs, particularly those representing stable continental region conditions and NGA-East-type models, results in higher predicted ground motions at short periods and provides a broader representation of epistemic uncertainty.

Additional contributions arise from the updated earthquake catalogue extended to 2026, revised magnitude of completeness and recurrence parameters, and refinements in the seismic source model, including zonation and treatment of the Øygarden Fault Zone. Minor differences may also be attributed to updates in computational implementation. Overall, the observed differences between the 2019 and 2026 results are consistent with expectations when incorporating updated datasets and modelling approaches and reflect current best practice for seismic hazard assessment in the Norwegian offshore region.

Despite these improvements, the hazard estimates remain subject to significant uncertainties. The earthquake catalogue, although updated and carefully processed, spans a relatively short observation period compared to the recurrence intervals of large earthquakes. This introduces uncertainty in the estimation of recurrence parameters, particularly for low-probability, high-magnitude events. Uncertainties in magnitude estimation, focal depth, and the identification of non-tectonic events further affect the robustness of the dataset.

Uncertainty also arises from the seismic source model. The delineation of area sources and the estimation of activity rates involve inherent subjectivity, particularly in regions of diffuse seismicity. The use of a regional b-value and the extrapolation of recurrence parameters to larger magnitudes introduce additional epistemic uncertainty. For the Øygarden Fault Zone, uncertainties in geometry, segmentation, slip rate, and maximum magnitude remain significant due to limited observational constraints.

Ground motion prediction represents another major source of uncertainty. None of the selected GMPEs have been developed specifically for Norwegian conditions, and their applicability relies on analogy with similar tectonic environments. While the use of multiple GMPEs within a logic-tree framework improves the representation of epistemic uncertainty, model selection and weighting remain partly subjective.

Finally, local topographic, site and basin amplification effects related to site conditions are not explicitly included in the hazard calculations and represent an additional source of uncertainty. These effects are addressed separately in the recommendations for further analysis and monitoring.

6.1 Conclusion

This study presents an updated site-specific PSHA for the U-864 wreck location, incorporating developments since the 2019 assessment, including an updated earthquake catalogue (to 2026), revised recurrence parameters, an updated source model, and a new GMPE logic tree consistent with recent Norwegian offshore studies.

The updated hazard estimates indicate moderately higher ground-motion levels compared to the 2019 results, particularly at short periods, while the overall spectral shape remains consistent. The increase is primarily driven by the updated ground-motion modelling and, to a lesser extent, by revisions to the seismicity model.

Despite remaining uncertainties, the updated model provides a more comprehensive and robust representation of seismic hazard at the U-864 site, reflecting current best practice and the incorporation of recent data and methodological developments.

Overall, the results confirm the general hazard level identified in the 2019 study, while providing an improved basis for engineering assessment and decision-making.

6.2 Recommendations for further analysis and monitoring

The current study has been carried out using the best available data and methods within the agreed scope. However, several aspects could be further refined or extended if additional data or resources became available. To further reduce uncertainties in the seismic hazard assessment for the U-864 site, additional analyses and improved data acquisition are recommended.

Enhanced seismic monitoring in offshore regions would significantly improve earthquake detection capability, event location accuracy, and focal depth resolution. The deployment of seismic stations in the vicinity of the U-864 site would provide valuable data for refining seismic source characterisation and improving future hazard assessments.

In 2021, NORSAR deployed a temporal nine-element seismic array on Holsnøy. The purpose of the installation was to improve background seismic characterisation in the proximity to CO2 storage operations (www.hordanet.no). Currently, the installation is about to become permanent, including power supply and data transmission, making it suitable for real-time continuous monitoring for the next 20-50 years. The data collected from this installation may also be used to monitor potential seismic, underwater landslide, explosion or other ground motion shaking in the proximity to the U-864 submarine. Such analysis could be conducted specifically aimed at that area and could provide real-time, continuous detection of any ground motion in that area. This could provide additional insurance, and early detection in case of any unexpected ground motion. Very local installation of fibreoptic cables could further improve such monitoring capabilities, and such feasibility can be evaluated on request.

The updated PSHA results are provided for bedrock reference conditions to maintain direct comparability with the 2019 study. However, the wreck site is underlain by marine sediments, and local site response may therefore modify ground motions at the seabed relative to bedrock conditions. Geotechnical investigations indicate that the seabed stratigraphy consists of a thin upper layer of gravelly sand overlying very soft clay and silt deposits, which in turn rest on moraine and bedrock (GeoPartner AS, 2010; NGI, 2013). The thickness of these sediment layers varies locally due to irregular bedrock topography and sediment infill between ridges.

Based on available bathymetric data, the seabed around the wreck is characterised by gentle slopes, with the bow section located on an approximately 15° slope and the stern section situated on a nearly flat seabed (GeoPartner AS, 2010). According to Eurocode 8 criteria (EN 1998-5:2004), slopes below approximately 15° do not result in significant topographic amplification; therefore, topographic effects are considered negligible (TAF ≈ 1.0). Similarly, bathymetric and geological observations indicate that the site is not located within a laterally extensive sedimentary basin. Instead, the seabed is characterised by irregular bedrock relief with localized sediment-filled depressions. Consequently, large-scale basin amplification effects are considered unlikely, although minor long-period effects cannot be entirely excluded.

Local soil amplification may occur due to the presence of soft sediments overlying stiffer material. Thin soft sediment layers may increase short to intermediate period ground motions, while thicker clay deposits (if present locally) may shift amplification towards longer periods and increase shaking duration. However, given the generally limited sediment thickness and the proximity of bedrock, amplification effects are expected to be moderate and highly site-specific.

First estimates of site effects may be obtained using Vs30 based site classification approaches. However, a more rigorous quantification would require dedicated site response analyses (1D or 2D numerical modelling) that account for local stratigraphy, stiffness contrasts, and nonlinear soil behaviour. Such analyses are recommended if a more detailed assessment of seabed ground motion is required for engineering purposes.

Previous geotechnical evaluations indicate that earthquake loading is not expected to critically affect the stability of the wreck or capping structure, with estimated permanent displacements remaining below approximately 20 cm even for rare design-level events (GeoPartner AS, 2010). Nevertheless, improved understanding of local site response would support more refined engineering assessments.

Overall, while topographic and basin amplification effects are expected to be negligible, local soil amplification remains a potential modifier of ground motions at the site. These effects are therefore identified as a key area for further investigation, together with improved offshore seismic monitoring, to enhance the robustness of future seismic hazard assessments.

7 References

Akkar, S., Sandıkkaya, M.A., Bommer, J.J., 2014. Empirical ground-motion models for point- and extended-source crustal earthquake scenarios in Europe and the Middle East. Bulletin of Earthquake Engineering 12, 359–387. https://doi.org/10.1007/s10518-013-9461-4

Atkinson, G.M., Boore, D.M., 2006. Earthquake Ground-Motion Prediction Equations for Eastern North America. Bulletin of the Seismological Society of America 96, 2181–2205. https://doi.org/10.1785/0120050245

Bell, R.E., Jackson, C.A.L., Whipp, P.S., Clements, B., 2014. Strain migration during multiphase extension: Observations from the northern North Sea. Tectonics 33, 1936–1963. https://doi.org/10.1002/2014TC003551

Bender, B., 1983. Maximum likelihood estimation of b values for magnitude grouped data. Bulletin of the Seismological Society of America 73, 831–851. https://doi.org/10.1785/bssa0730030831

Bindi, D., Cotton, F., Kotha, S.R., Bosse, C., Stromeyer, D., Grünthal, G., 2017. Application-driven ground motion prediction equation for seismic hazard assessments in non-cratonic moderate-seismicity areas. J. Seismol. 21, 1201–1218. https://doi.org/10.1007/s10950-017-9661-5

Bindi, D., Pacor, F., Luzi, L., Puglia, R., Massa, M., Ameri, G., Paolucci, R., 2011. Ground motion prediction equations derived from the Italian strong motion database. Bulletin of Earthquake Engineering 9, 1899–1920. https://doi.org/10.1007/s10518-011-9313-z

Boore, D., 2015. Point-source stochastic-method simulations of ground motions for the PEER NGA-East project, Pacific Earthquake Engineering Research Center (PEER).

Bungum, H., 2007. Numerical modelling of fault activities. Comput. Geosci. 33, 808–820. https://doi.org/10.1016/j.cageo.2006.10.011

Bungum, H., Alsaker, A., Kvamme, L.B., Hansen, R.A., 1991. Seismicity and seismotectonics of Norway and nearby continental shelf areas. Geodesy and Gravity Tectonophysics 96, 2249–2265. https://doi.org/https://doi.org/10.1029/90JB02010

Cauzzi, C., Faccioli, E., Vanini, M., Bianchini, A., 2015. Updated predictive equations for broadband (0.01–10 s) horizontal response spectra and peak ground motions, based on a global dataset of digital acceleration records. Bulletin of Earthquake Engineering 13, 1587–1612. https://doi.org/10.1007/s10518-014-9685-y

Cornell, C.A., 1968. Engineering seismic risk analysis. Bulletin of the Seismological Society of America 58, 1583–1606.

EN 1998-5:2004, n.d. Eurocode 8—design of structures for earthquake resistance, part 5: Foundations, retaining structures and geotechnical aspects. Brussels.

Esteva, L., 1963. Regionalizacion sismica de la Republica Mexicana. Revista Sociedad Mexicana do Ingenieria Sismica 1, 31–35.

Faleide, J.I., Bjørlykke, K., Gabrielsen, R.H., 2015. Geology of the norwegian continental shelf, in: Petroleum Geoscience: From Sedimentary Environments to Rock Physics, Second Edition. pp. 603–637. https://doi.org/10.1007/978-3-642-34132-8_25

Fossen, H., Hurich, C.A., 2005. The Hardangerfjord Shear Zone in SW Norway and the North Sea: a large-scale low-angle shear zone in the Caledonian crust. J. Geol. Soc. London. 162, 675–687.

Gabrielsen, R.H., Færseth, R.B., 1989. The inner shelf of North Cape, Norway and its implications for the Barents Shelf-Finmark Caledonide boundary. A comment. Norsk Geologisk Tidsskrift 69, 57–62.

GeoPartner AS, 2010. Submarine Wreck U-864. Encapsulation of Wreck and Capping of Contaminated Seabed. Geotechnical Design and Guidelines for Installation.

Gutenberg, B., Richter, C.F., 1956. Magnitude and Energy of Earthquakes. Annali di Geofisica 9, 1–15.

Hashash, Y.M.A., Ilhan, O., Harmon, J.A., Parker, G.A., Stewart, J.P., Rathje, E.M., Campbell, K.W., Silva, W.J., 2020. Nonlinear site amplification model for ergodic seismic hazard analysis in Central and Eastern North America. Earthquake Spectra 36, 69–86. https://doi.org/10.1177/8755293019878193

Havskov, J., Bungum, H., 1987. Source parameters for earthquakes in the northern North Sea. Norsk Geologisk Tidsskrift 67.

Hicks, E.C., Bungum, H., Lindholm, C.D., 2000. Stress inversion of earthquake focal mechanism solutions from onshore and offshore Norway. Norsk Geologisk Tidsskrift 80. https://doi.org/10.1080/00291960051030545

Jonassen, P., 2015. Fault analysis based on 3D seismic data from the northern Horda Platform. University of Oslo.

Lindholm, C., Bungum, H., Ghione, F., Meslem, A., Huang, C., Oye, V., 2025. Earthquakes and Seismic Hazard for Norway and Svalbard. J. Seismol. https://doi.org/https://doi.org/10.1007/s10950-024-10270-z

Lindholm, C., Roth, M., Bungum, H., Faleide, J.I., 2005. Probabilistic and deterministic seismic hazard results and influence of the sedimentary Møre Basin, NE Atlantic. Mar. Pet. Geol. 22, 149–160.

Lindholm, C.D., Bungum, H., Hicks, E., Villagran, M., 2000. Crustal stress and tectonics in Norwegian regions determined from earthquake focal mechanisms. Geol. Soc. Spec. Publ. 167. https://doi.org/10.1144/GSL.SP.2000.167.01.17

Møllegaard, E., 2000. Seismotektonikk i nordlige Nordsjø. Universitetet i Oslo.

NGI, 2013. U-864 2013 Soil survey Geotechnical Report.

NORSAR, 2025. Site-Specific Probabilistic Seismic Hazard Assessment (PSHA) for Grane. Confidential report.

NORSAR, 2022. Site-specific Probabilistic Seismic Hazard Assessment (PSHA) for NOA-Krafla submarine cable from Samnanger, Norway. Kjeller, Norway. Confidential report.

NORSAR, 2020. Seismic Zonation and Earthquake loading for Norway and Svalbard; Load estimates as basis for Eurocode 8 applications. Kjeller, Norway.

NORSAR, 2019. Site-Specific Seismic Hazard Study for the Submarine Wreck U-864 Location, Norway. Kjeller, Norway.

NORSAR, NGI, 1998. Development of a seismic zonation for Norway. Report for Norwegian Council for Building Standardization. Kjeller, Norway.

NORSOK N-003, 2017. Actions and action effects N-003. Oslo, Norway.

Olesen, O., Janutye, I., Michalek, J., Keiding, M., 2018. Neotectonics in Nordland - Implications for petroleum exploration (NEONOR2). NGU Report No. 2018.010.

Ordaz, M., Martinelli, F., D'Amico, V., Meletti, C., 2013. CRISIS2008: A flexible tool to perform probabilistic seismic hazard assessment. Seismological Research Letters 84. https://doi.org/10.1785/0220120067

Ordaz, M., Salgado-Gálvez, M.A., Giraldo, S., 2021. R-CRISIS: 35 years of continuous developments and improvements for probabilistic seismic hazard analysis. Bulletin of Earthquake Engineering 19. https://doi.org/10.1007/s10518-021-01098-w

Pezeshk, S., Zandieh, A., Campbell, K.W., Tavakoli, B., 2018. Ground-motion prediction equations for central and eastern north America using the hybrid empirical method and NGA-west2 empirical ground-motion models. Bulletin of the Seismological Society of America 108, 2278–2304. https://doi.org/10.1785/0120170179

Ramberg, I.B., Bryhni, I., Nøttvedt, A., 2007. Landet blir til - Norges geologi. GeologiskNyt 17. https://doi.org/10.7146/gn.v0i4.3409

Rietbrock, A., Edwards, B., 2019. Update of the UK stochastic ground motion model using a decade of broadband data. Greenwich, United Kingdom.

Smirnova, K., 2019. Potential Seismogenic Faults in Norway. University of Bergen.

Stewart, J.P., Parker, G.A., Atkinson, G.M., Boore, D.M., Hashash, Y.M.A., Silva, W.J., 2020. Ergodic site amplification model for central and eastern North America. Earthquake Spectra 36, 42–68. https://doi.org/10.1177/8755293019878185

Van Stiphout, T., Zhuang, J., Marsan, D., 2012. Seismicity Declustering. Community Online Resource for Statistical Seismicity Analysis. https://doi.org/10.5078/corssa

Weatherill, G., Cotton, F., 2020. A ground motion logic tree for seismic hazard analysis in the stable cratonic region of Europe: regionalisation, model selection and development of a scaled backbone approach. Bulletin of Earthquake Engineering 18, 6119–6148. https://doi.org/10.1007/s10518-020-00940-x

Wells, D.L., Coppersmith, K.J., 1994. New empirical relationships among magnitude, rupture length, rupture width, rupture area, and surface displacement. Bulletin of the Seismological Society of America 84, 974–1002.

Wood, M., Woo, G., 1987. The Historical Seismicity of the Norwegian Continental Shelf. Earthquake Loading on the Norwegian Continental Shelf (ELOCS). Oslo.

Yenier, E., Atkinson, G.M., 2015. Regionally adjustable generic ground-motion prediction equation based on equivalent point-source simulations: Application to central and eastern North America. Bulletin of the Seismological Society of America 105, 1989–2009. https://doi.org/10.1785/0120140332

Youngs, R.R., Coppersmith, K.J., 1985. Implications of fault slip rates and earthquake recurrence models to probabilistic seismic hazard estimates. Bulletin of the Seismological Society of America 75, 939–964.

Report Documentation Page

Report Number: 26-001	NORSAR Project No. 10341	No. of pages: 41	Confidential report	Date: 06/05/2026
Title:	Update of the 2019 Site-Specific Seismic Hazard Study for submarine U-864 location			
Client:	Kystverket			
Client ref.	Lill Veronika Benjaminsen			
Project Manager:	Federica Ghione			
Authors / Prepared by:	Federica Ghione, Volker Oye			
Submitted to:	Kystverket, Postboks 1502, 6025 Ålesund, Norway			
Approved by:	Name:	Signature:	Date:	
	Head of Department Volker Oye		06.05.2026	

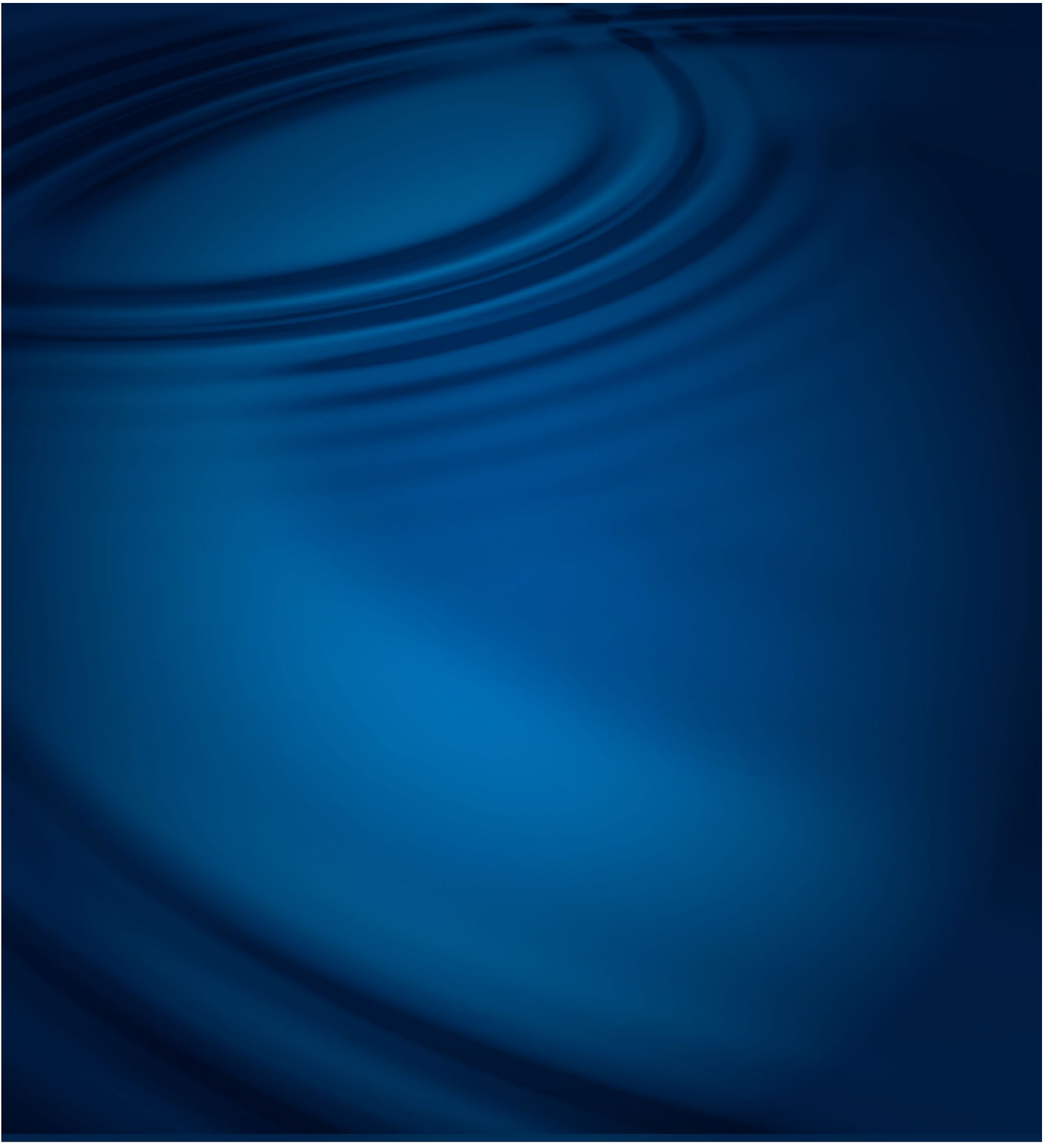

NORSAR